AFCRL-63-890

THE UNIVERSITY OF MICHIGAN
COLLEGE OF LITERATURE, SCIENCE, AND THE ARTS
Department of Physics

Technical Report No. 2

THE DETERMINATION OF THE HINDERED MOTION IN HYDROGEN PEROXIDE FROM ITS FAR INFRARED SPECTRUM

Robert H. Hunt

ORA Project 03640

Contract No. AF19(604)-6125
Project 8603
Task 860301

under contract with:

AIR FORCE CAMBRIDGE RESEARCH LABORATORIES
OFFICE OF AEROSPACE RESEARCH
UNITED STATES AIR FORCE
BEDFORD, MASSACHUSETTS

administered through:

OFFICE OF RESEARCH ADMINISTRATION ANN ARBOR

June 1963

This report was also a dissertation submitted in partial fulfillment of the requirements for the degree of Doctor of Philosophy in The University of Michigan, 1963.

TABLE OF CONTENTS

LIST OF TABLES

LIST OF FIGURES

ABSTRACT

The torsional oscillation between the two OH groups of the hydrogen peroxide molecule has been investigated by a study of the absorption spectrum of the vapor in the far infrared. A one meter focal length vacuum grating monochromator was used to scan the region from 15 to 700 cm^{-1} with an average resolution of 0.3 cm^{-1}. The spectrum could be analyzed into a number of perpendicular type bands of which only the Q branches ($\Delta K = \pm 1$, $\Delta J = 0$ transitions) could be identified. The centers of the seven bands that could be recognized were at 11.43, 116.51, 198.57, 242.76, 370.70, 521.68, and 557.84 cm^{-1}. These bands result from transitions between different states of the internal rotation and their identification made it possible to construct the internal rotation energy level scheme complete through the first five excited states. Relative to the ground state, these levels occur at 11.43, 254.2, 370.7, 569.3, and 775.9 cm^{-1}.

Leacock and Hecht have concurrently developed a treatment of the internal motion, expressing the hindering potential function as a Fourier series in x (where x is the dihedral angle between the two OH groups). The Hamiltonian for the internal motion was solved for its eigenvalues on an IBM 709 computer. The observed internal rotation levels and transsitions were fitted to better than 1 cm^{-1} with the hindering potential function $V(x) = 993 \cos x + 636 \cos 2x + 44 \cos 3x$ (where the coefficients are expressed in cm^{-1}). This hindering potential has a cis barrier of 2460 cm^{-1}, a trans barrier of 386 cm^{-1}, and a minimum value at 111.5° from the cis configuration. In addition, a number of anomalies in the spectra were quantitatively accounted for by the theory.

I. INTRODUCTION

Hydrogen peroxide is the simplest molecule having a possible internal rotation motion—a motion that can be described as a torsional oscillation of one OH group with respect to the other. Penney and Sutherland (1) concluded from consideration of the electron structure of the molecule that it should have a non-planar equilibrium configuration as shown in Figure 1 due to maxima in the internal potential energy at the cis ($x=0$) and trans ($x=\pi$) positions. They predicted that the equilibrium value of x should be in the neighborhood of 90°, and that the angle ϵ should be about 100°. The heights of the cis and trans barriers were estimated to be 8000 and 4000 cm^{-1}, respectively.

An overtone vibration band of H_2O_2 vapor observed in the photographic infrared by Zumwalt and Giguere (2) showed evidence of being doubled. This led them to suggest that the potential maxima must be considerably lower than predicted by Penney and Sutherland if the doubling was due to hindered internal motion of the OH groups. Later investigations of the vibrational spectrum of H_2O_2 by Giguere and his co-workers (3,4,5) fairly well established the molecular form predicted by Penney and Sutherland. However, their spectral resolution was not sufficient to show any fine structure that would give information as to the internal rotation of the molecule.

More conclusive evidence of level splitting due to internal rota-

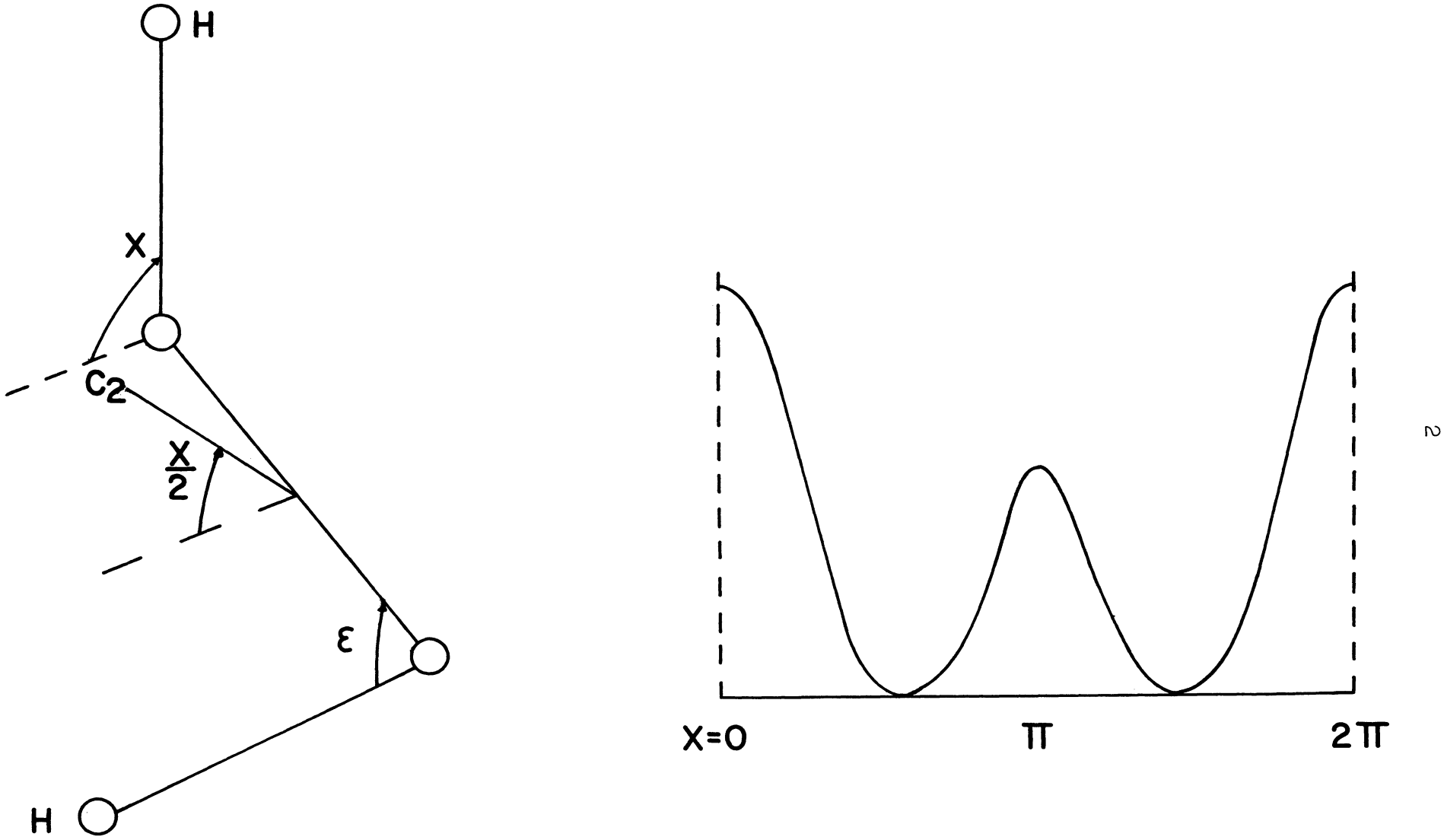

Figure 1. Structure of H_2O_2 and form of the hindering potential.

tion was obtained by Massey and Bianco (6) from microwave absorption measurements. Level splittings of 11 to 22 cm^{-1} were necessary to explain their data which was essentially two transitions whose J values were determined from their Stark effects. However, it was not certain whether this splitting occurred in the ground state or some excited state of the internal motion. As pointed out by Massey and Hart (7) in a later paper, more information is needed to make any definite statements about the hindering potential. An attempt to obtain the microwave spectrum of D_2O_2 was complicated by the presence of DOOH as an impurity in the sample and the observed lines could not be definitely assigned to either molecule (8).

The work reported here was undertaken to determine the hindering potential from the far infrared absorption spectrum which arises from transitions between different internal rotation states. The microwave absorption work of Massey et al., showed the molecule to have a large dipole moment (2.26 Debye). Consequently, the far infrared absorption was expected to be reasonably intense. Bain and Giguère (5) had observed absorption attributable to such transitions in the spectral region 700 to 400 cm^{-1} but the low resolution of their prism spectrograph precluded an accurate analysis of the bands. In the work to be described, a vacuum grating spectrograph was used in the region 15 to 700 cm^{-1} with an average resolution of about 0.3 cm^{-1}. The region 15 to 150 cm^{-1} was investigated first and some results of this work were

reported in 1961 (9). Among other things, it was shown that the splitting inferred from the microwave data was that of the ground state. While the remainder of this work was in progress, Chin and Giguere (10) extended prism observations to 300 cm^{-1}. Also, during this period Redington, Olsen, and Cross (11) published results of a moderately high resolution study of the near infrared bands in H_2O_2. Their detailed band analysis yielded the first accurate set of ground state rotational constants.

II. EXPERIMENTAL ARRANGEMENT AND PROCEDURE

The spectrograph used in this investigation was that designed and built by Randall and Firestone (12) but with new fore optics and detection systems. Prior to this investigation, the effective long wavelength range of this instrument was not much beyond 100 microns. This was because the method employed to eliminate signals due to higher order radiation depended primarily on a single reflection from a material exhibiting Restrahlen or selective reflection. No Restrahlen materials are available suitable for use beyond 200 microns and those available in the 100 to 200 micron range are not very efficient. Since many of the hydrogen peroxide transitions of interest occur at wavelengths longer than 100 microns, a new set of fore optics was constructed in which the higher spectral orders of shorter wavelengths were scattered by small reflection gratings. Figure 2 is a schematic diagram of the optical path of the instrument. G_1 and G_2 are 2" by 3" gratings which receive radiation rendered parallel by the spherical mirror M_6.

The fore optics are aligned with mirrors in place of G_1 and G_2. With G_1 and G_2 in place then, only radiation which is not dispersed by them will enter the spectrograph. The grating spacings are chosen so that wavelengths longer than the minimum wavelength desired, λ_{min}, cannot be dispersed. A single grating will not produce complete dis-

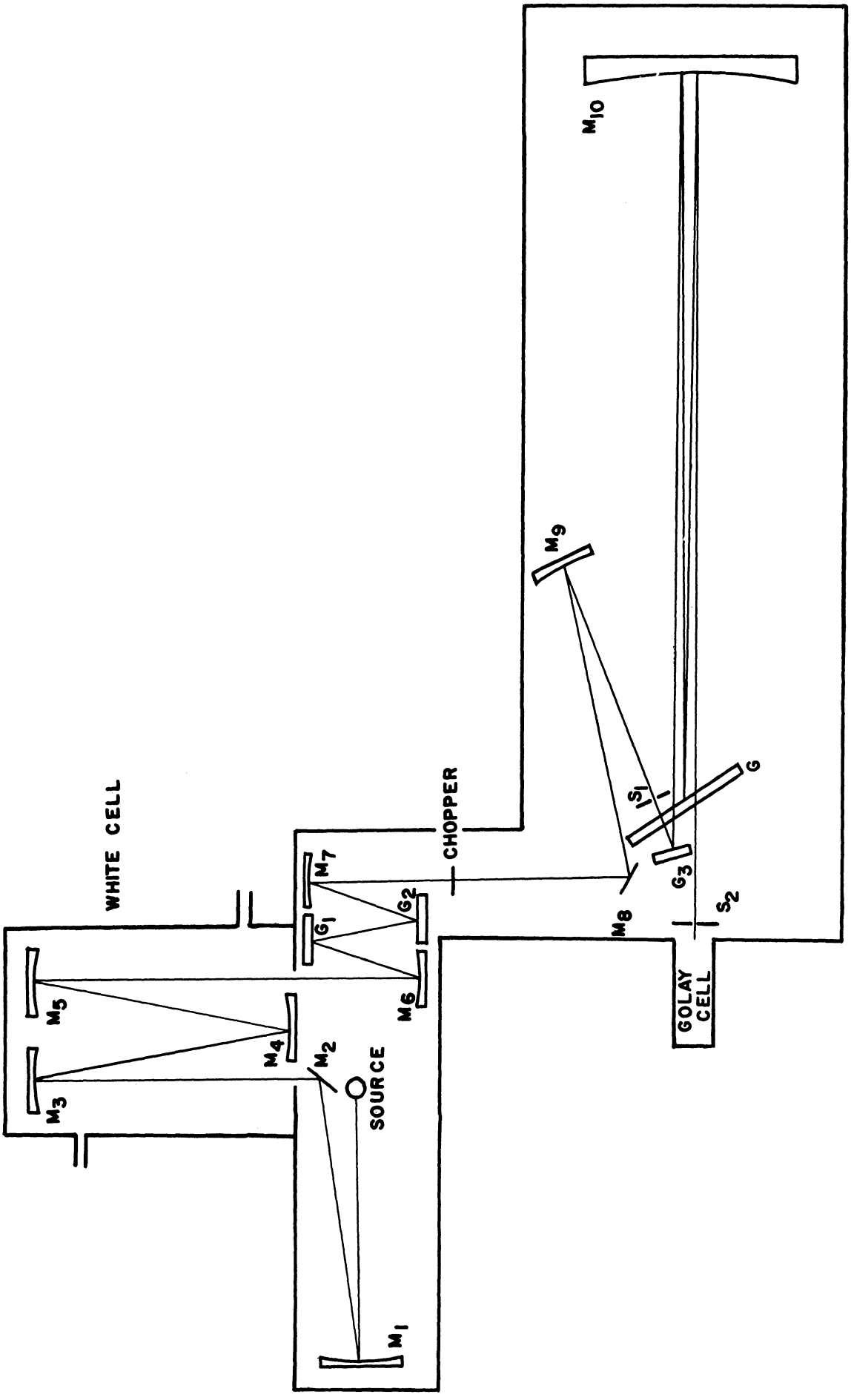

Figure 2. Diagram of spectrograph and fore optics.

persion for $\lambda < \lambda_{min}$, particularly for that polarization of the radiation with its electric vector parallel to the grooves of the grating. By using two gratings whose rulings are perpendicular to each other, a high degree of dispersion for both polarizations is provided. Several sets of crossed gratings G_1 and G_2 with different spacings are necessary to cover the spectral range of the instrument because each set can provide filtration for only one octave of the spectrum, λ_{min} to $2\lambda_{min}$. Upon adding yet a third filtration grating G_3, this one in the position originally occupied by the Restrahlen plate, with its rulings crossed with those of the main grating, it was possible to scan through the blaze of the main grating without a noticeable increase in impurity in the spectrum. No trace of higher order radiation could be observed in any of the spectra obtained. Checks made by inserting KI and NaCl in the beam showed less than 5% impurity when operating in regions beyond their long wavelength transmission cut-off. A glass bladed beam chopper was used for all regions of the spectrum.

The fore optics were designed to accomodate two types of radiation sources. For the region 700 to 100 cm^{-1} the source used was an electrically heated platinum strip 1" x 1/4 " x .005" coated with a mixture of carborundum and water glass. This coating was found to increase the emissivity of the source by more than a factor of 2. For the region 100 to 15 cm^{-1} a high pressure Hg discharge lamp was used as a source. The largest output was obtained from a Hanovia Eh-1 400

watt lamp with, of course, the outer glass envelope removed. It was necessary to water cool the Hg source housing.

The absorption cell was a White type multiple reflection cell made with only aluminum and glass components in order to retard the decomposition of the peroxide. The mirrors had a 40 cm radius of curvature and path lengths of integer multiples of 160 cm could be selected. Cell windows were 6 mil polyethylene, and were about 90% transparent throughout the range 15 to 700 cm^{-1}. In the region 15 to 100 cm^{-1} where the Hg lamp source was used, it was necessary to replace the window in the proximity of the lamp with 1 mm of Teflon. McCubbin (13) indicates that Teflon of this thickness transmits about 70% at 100 cm^{-1} and about 90% at 15 cm^{-1}. The windows were sealed to the cell by first gluing them down with G. C. Vinylite cement and then screwing a retaining plate over them. Since this is a vacuum spectrograph, the cell windows are subject only to the pressure of the sample in the cell so that thin windows of little mechanical strength can be used. The cell could be heated to moderate temperature (70°C or so).

The radiation detector was a Golay cell fitted with a brass cone designed to accept radiation from a one inch long section of the exit slit and condense it down to the sensitive area of the Golay cell which is 3 mm in diameter. The Golay cell was enclosed in a vacuum tight can which was sealed off from the spectrograph proper by a window of suitable transmission for the region being scanned. This can

was flushed with dry nitrogen to remove the water vapor from the two inch length of the cone. In this way, the possibility of damaging the Golay cell by operating it in a vacuum was avoided. Because a Golay cell is extremely sensitive to vibrations, it was necessary to shock mount the cell in its housing by means of sponge rubber.

The initial portion of the spectrum, 15 to 100 cm^{-1}, was obtained using a Golay cell with a crystal quartz window and a similar window on the housing. The remaining portion of the spectrum was recorded using a diamond window cell purchased during the course of the work. Unlike quartz, diamond has no absorption bands in the far infrared and so is suitable for the entire region investigated here. Beyond 100 microns, however, there is some slight advantage in using the quartz cell due to its lower reflection losses. For the region below 100 microns the quartz window on the cell housing was replaced with 12 mil polyethylene. This thickness was sufficient to withstand atmospheric pressure over the 1" x 1/4" area.

The radiation was chopped at 10 cycles per second and the signal from the Golay cell was fed into a single stage pre-amplifier and then into the amplifier and synchronous detector unit supplied by Eppley Laboratories. The output from the synchronous detector was displayed on a Leeds and Northrup chart recorder.

To obtain a reduced noise level and maximum resolution, additional non-electrolytic capacitors were added to the RC integration network

of the Eppley unit extending the choice of time constants to include 18, 32, 70, or 105 seconds. It was found that a scanning speed per resolution interval corresponding to three times the time constant employed resulted in very little information loss. In practice, a response time of 105 seconds is tediously long and its use was restricted to the region from 15 cm^{-1} to 30 cm^{-1}. The response times used in other spectral regions are listed as part of Table I.

Resolution between 0.2 cm^{-1} and 0.4 cm^{-1} throughout the region 15 to 700 cm^{-1} was maintained through the use of nine different main gratings. The number of lines per inch of each grating and the region in which it was used is given in Table I along with the purification gratings employed. The need for such a large number of gratings is a consequence of the almost fifty-fold wavelength change encompassed in this investigation and the necessity of working at large grating angles to maintain good resolution. All of the gratings used in this work were ruled at The University of Michigan. Most of the main gratings listed are the original 10" x 18" gratings ruled for this instrument. The remaining gratings, including all the purification gratings, were ruled while this work was in progress.

The experimental difficulties encountered in obtaining detailed hydrogen peroxide spectra arise primarily from the tendency of the vapor to decompose upon contact with many substances. Since one of the decomposition products is water, special care must be taken in most re-

gions of the H_2O_2 spectrum to reduce the absorption of water vapor formed by decomposition to a tolerable level. The following procedure was found to be successful in contending with the problem of water vapor whose pure rotation spectrum extends throughout the region of investigation here.

TABLE I

GRATINGS AND TIME CONSTANTS USED IN THE REGION 700 TO 15 CM^{-1}

Region (cm^{-1})	Main Grating	G_1	G_2	G_3	Time Constant (sec)
700-560	2400	2400	1800	Mirror	18
560-450	1440	2400	1440	1800	18
450-320	1440	1440	1440	1800	18
320-250	900	1440	757	1800	32
250-200	900	757	757	1800	32
200-150	600	757	757	1800	32
150-140	600	450	378	1800	32
140-100	400	450	378	1800	32
100- 75	160	450	378	320	32
75- 47	160	232	194	240	32
47- 40	80	232	194	240	32
40- 30	80	116	100	120	70
30- 20	25	116	100	120	105
20- 15	15	66	66	120	105

Grating spacings are in lines per inch.

As mentioned previously, the absorption cell was constructed of aluminum and glass with polyethylene or Teflon windows. Hydrogen peroxide does not react strongly with polished aluminum as evidenced by the lack of deterioration of the aluminum surfaced mirrors contained in

the cell even after many hours of exposure to hydrogen peroxide vapor. Decomposition within the cell was rapid enough, however, to necessitate the use of a continuous flow technique in which the peroxide vapor was pumped through the cell from a reservoir heated to maintain the liquid peroxide close to room temperature (25°C) where its vapor pressure is about 2 mm of Hg (11). The cell was heated somewhat above room temperature to prevent condensation. The peroxide sample as obtained from the Buffalo Electrochemical Corporation was 98% pure. Absorption cell paths were; 4.8 meters from 700 to 450 cm^{-1}, 1.6 meters from 450 to 30 cm^{-1}, and 3.2 meters from 30 to 15 cm^{-1}.

All traces of atmospheric water absorption were removed by evacuating the spectrograph to a pressure of less than 100 microns of Hg and flushing the Golay housing with dry nitrogen. The most water free H_2O_2 spectra were obtained after the cell had been in use for some time and had become "acclimatized" to the peroxide. To obtain an accurate estimate of the contribution of water to the H_2O_2 spectrum, it was necessary to run the water vapor spectrum throughout the entire region under similar operating conditions. Only a few of the strongest water lines can be recognized in the H_2O_2 spectrum and it is believed that no H_2O_2 absorption of any appreciable intensity has been attributed to H_2O and conversely that no strong H_2O line has been assigned to H_2O_2. At one or two points in the spectrum where moderately strong H_2O and H_2O_2 absorptions overlap, there is a considerable uncertainty as to their relative contributions.

A reproduction of a recorder trace is shown in Figure 3 to illustrate a typical scan. Two complete scans were made of the entire region and the spectra were found to be very reproducible. Owing to irregularity in the energy envelope in the 15 cm^{-1} to 100 cm^{-1} region a set of background runs also had to be made there.

To determine absorption frequencies blips were placed on the recording chart to correspond to angles read from the grating circle. After each run the angular position of the central image was recorded under the same operating conditions. The grating constants were determined by the observation of absorption lines of HCN, H_2O, and CO. Estimated errors in determining the positions of unknown sharp lines are:

$\pm$ .05 cm^{-1} for lines between 700 and 450 cm^{-1},

$\pm$ .03 cm^{-1} for lines between 450 and 200 cm^{-1},

$\pm$ .02 cm^{-1} for lines between 200 and 15 cm^{-1}.

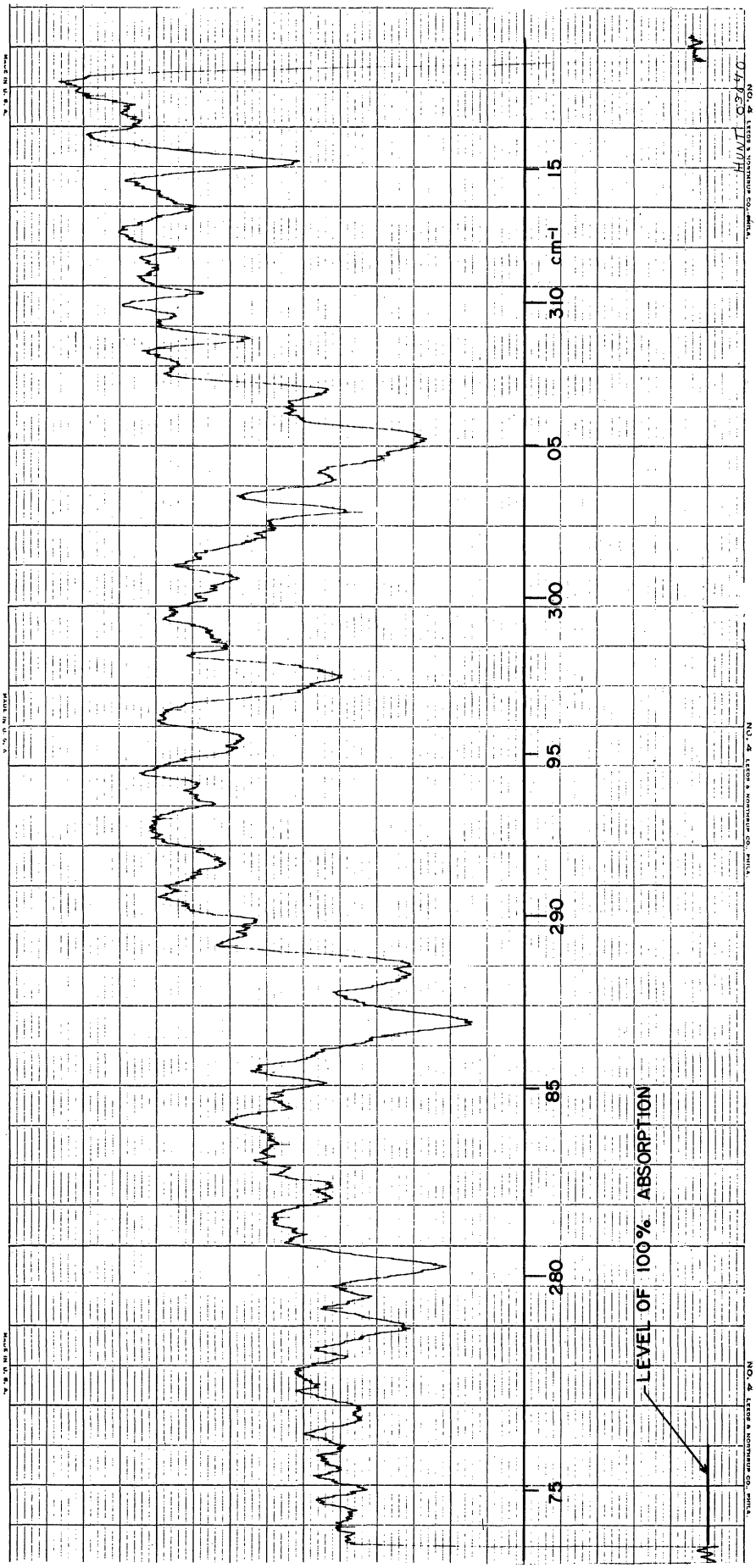

Figure 3. Recorder trace of H_2O_2 absorption.

III. THEORY OF HINDERED INTERNAL ROTATION IN HYDROGEN PEROXIDE

Hydrogen peroxide belongs to the most general class of internal rotators in that neither group has its center of mass on the axis of mutual rotation. Burkhard (14) has written out the form of the matrix elements of the Hamiltonian for the most general molecule in this class. While these matrix elements could be reduced to the somewhat more simple case of hydrogen peroxide, Leacock and Hecht (15) have shown that the problem of hydrogen peroxide is more conveniently formulated by putting the Hamiltonian in a form in which there are no cross terms in the overall and internal angular momenta. The next few pages are an outline of their theoretical treatment which was developed concurrently with the latter stages of this experimental work.

The molecule is taken to be a rigid structure except for the possibility of hindered internal rotation. The problem is then one of four degrees of freedom, three Euler angles describing the overall rotation of the molecule plus the angle describing the relative orientation of the OH groups. This is an approximation which neglects interaction of the higher frequency normal vibrations with the internal and overall rotation. The lowest frequency normal vibration in hydrogen peroxide occurs at nearly 900 cm^{-1} or several hundred wavenumbers higher than any observed rotational frequencies so that the neglect of rotation-vibration interactions should not lead to serious errors. The gen-

erally good agreement between theory and experiment shows that in most cases the effects of these interactions are small although not negligible. More will be said about such effects later.

It is assumed that the hindering potential $V(x)$ can be well represented by the first few terms in its Fourier expansion, $V(x) = V_1 \cos x + V_2 \cos 2x + V_3 \cos 3x + \ldots$, with the first two terms predominant owing to the requirement that there be potential maxima in the cis and trans positions.

The cis barrier is shown larger than the trans barrier in Figure 1. The impossibility of V_{CIS} being less than V_{TRANS} will become evident when the nature of the internal levels for these two cases and the experimental results have been considered.

An exact expression for the kinetic energy of this four dimensional problem is first obtained referred to a coordinate system fixed at the center of mass of the molecule with the X axis along the C_2 symmetry axis and the Z axis parallel to the O-O bond. Straightforward calculations yield:

$$2T = \frac{1}{AG-F^2}\left\{G P_x^2 + 4A p_x^2 - 4F p_x P_x\right\} + \frac{1}{BC-D^2}\left\{C P_Y^2 + B P_Z^2 - 2D P_Y P_Z\right\}$$

P_X, P_Y, P_Z, are the components of the angular momentum of overall rotation referred to the axes defined above. p_x is an angular momentum as-

sociated with the internal rotation. x is the internal angle shown in Figure 1.

$$A = I_{xx} = A_o + A' \sin^2 \frac{x}{2}$$

$$B = I_{YY} = A_o + C_o\left(1 - \sin^2 \frac{x}{2}\right)$$

$$C = I_{ZZ} = C_o + C' \sin^2 \frac{x}{2}$$

$$D = I_{YZ} = D_o \sin \frac{x}{2}$$

$$F = D_o \cos \frac{x}{2}$$

$$G = C_o + C'\left(1 - \sin^2 \frac{x}{2}\right)$$

where

$$A_o = \frac{M r_1^2}{2} + 2m\left(\frac{r_1}{2} - r_2 \cos \epsilon\right)^2$$

$$A' = 2m\left(r_2^2 \sin^2 \epsilon\right)$$

$$C_o = 2\mu\left(r_2^2 \sin^2 \epsilon\right)$$

$$C' = 2\left(\frac{m^2}{M+m} r_2^2 \sin^2 \epsilon\right)$$

$$D_o = 2m\left(r_2 \sin \epsilon\right)\left(r_2 \cos \epsilon - \frac{r_1}{2}\right)$$

$$\mu = \frac{m M}{m + M}$$

with

m = mass of hydrogen nucleus

M = mass of the oxygen nucleus

r_1 = O-O bond length

r_2 = O-H bond length

ϵ = O-O-H angle

The following contact transformation is then applied to eliminate the cross term in the momenta, $p_X P_X$, which occurs due to the product of inertia D.

$$x = x'$$

$$p_x = p'_x + \frac{F}{2A} P'_x$$

$$P_x = P'_x$$

$$P_Y = \cos U(x) P'_Y + \sin U(x) P'_Z$$

$$P_Z = -\sin U(x) P'_Y + \cos U(x) P'_Z$$

where

$$U(x) = \frac{-D_o}{(A_o A')^{1/2}} \tan^{-1} \left\{ \left(\frac{A'}{A_o}\right)^{1/2} \sin \frac{x}{2} \right\}$$

The exact kinetic energy in this new coordinate system is an exceedingly complicated function of x. However, because the mass of the hydrogen nucleus is only one-sixteenth the mass of the oxygen nucleus, the moments of inertia A, B, and C are dominated by terms independent of x. Further, D, F, and G, although strongly x dependent, are much smaller than A, B, or C. These facts make it feasible to expand the coefficients of the momenta and retain only the first few terms. When this is done, the kinetic energy can be written in the rather simple form:

$$T = \beta(x)\left[P_x'^2 + P_Y'^2 + P_z'^2\right] + \nu(x) P_z'^2 + P_x'^2 \alpha(x) +$$

$$\gamma(x)\left[P_x'^2 - P_Y'^2\right] + \delta(x)\left[P_Y' P_z' + P_z' P_Y'\right]$$

where

$$\beta(x) = \beta_0 + \beta_1 \cos x + \beta_2 \cos 2x + \ldots$$

$$\nu(x) = \nu_0 + \nu_1 \cos x + \nu_2 \cos 2x + \ldots$$

$$\gamma(x) = \gamma_0 + \gamma_1 \cos x + \gamma_2 \cos 2x + \ldots$$

$$\delta(x) = \delta_1 \sin^3 \frac{x}{2} + \ldots$$

$$\alpha(x) = \alpha_0 + \alpha_1 \cos x + \alpha_2 \cos 2x + \ldots$$

(Hereafter, the primes on the new momenta will be dropped). The coefficients in these latter expansions are given in terms of A_0, A', C_0, C', and D_0. The expressions are quite involved and will not be given here. The best values of the parameters r_1, r_2 and ϵ have been determined spectroscopically by Redington et al., (11) using a simplified theory of the molecule.

They quote; $r_1 = 1.475\ A^\circ \pm .004\ A^\circ$, $r_2 = 0.950\ A^\circ \pm .005\ A^\circ$, $\epsilon = 94.8^\circ \pm 2^\circ$. As will be discussed later, the present theory requires no significant modification of these values to fit the experimental data. The corresponding values of the coefficients in cm^{-1} are:

$$\beta(x) = 0.8589 + 0.0025 \cos x + 0.0008 \cos 2x$$

$$\nu(x) = 9.158 - 0.103 \cos x + 0.008 \cos 2x$$

$$\gamma(x) = 0.0005 + 0.0367 \cos x + 0.0002 \cos 2x$$

$$\alpha(x) = 39.94 + 0.25 \cos x + 0.04 \cos 2x$$

$$\delta(x) = 0.09 \sin^3 \frac{x}{2}$$

All further terms in these expansions are negligible for present purposes. The magnitudes of the expansion coefficients demonstrate that the internal rotation and the overall rotation are not strongly coupled in the new coordinate system.

The matrix of the Hamiltonian T + V(x) is now written out using the basis wavefunctions $\psi_{JK_{\pm}M} \cdot M_{n\tau}(x)$, where $\psi_{JK_{\pm}M}$ are the symmetrized symmetric top functions $\frac{1}{2^{1/2}} \left\{ \psi_{JKM} \pm \psi_{J-KM} \right\}$, and $M_{n\tau}(x)$ are the eigenfunctions of the equation

$$\{p_x^2 \alpha(x) + V_1 \cos x + V_2 \cos 2x + V_3 \cos 3x + \ldots - W\} M(x) = 0.$$

This equation is essentially the same as that used by Koehler and Dennison (16) in their treatment of hindered internal rotation in methyl alcohol. Its solutions are of the form $M(x) = e^{i\sigma x} P(x)$ where P(x) is periodic with period 2π. σ is determined by the boundary conditions relating the overall rotation of the molecule and the internal rotation. In the case of hydrogen peroxide $\sigma = -1/2$ K. Several investigators (7,11,17) have discussed the nature of the solutions to the internal wave equation for hydrogen peroxide. P(x) is conveniently expanded in a Fourier series and the general form of M(x) written as:

$$M(x) = e^{-i\frac{K}{2}x} \sum_{N=-\infty}^{\infty} A_N e^{iNx}$$

The forms of M(x) with the correct symmetry to factor the energy matrix of the internal motion can be found by examining the invariances of the Hamiltonian.

The total Hamiltonian is unchanged by overall rotation and inversion through the center of mass. Its eigenfunctions can be chosen so that they either do or do not change sign under these operations. With the help of Figure 4, which shows a view of hydrogen peroxide looking down the O-O bond, it can be seen that inversion through the center of mass can be accomplished either by a reflection of the molecule through the trans plane followed by overall rotation by π about the C_2 (or X) axis; or by a reflection through the cis plane plus an overall rotation about the Z axis by π followed by a rotation by π about the C_2 axis. Tunneling through either the cis or trans barrier is therefore an inversion motion in the usual sense and the level splitting produced is an inversion splitting. The wavefunctions ψ_{JKM} transform as $(-1)^K \psi_{JKM}$ under C_2^Z $(\phi \rightarrow \phi + \pi)$. Reflections through the cis plane $(\sigma_{CIS} = x \rightarrow -x)$ or the trans plane $(\sigma_{TRANS} = x \rightarrow 2\pi - x)$ do not affect ψ_{JKM}, but M(x) must be either symmetric (s) or antisymmetric (a) under these operations since they leave the internal Hamiltonian $p_x^2\, \alpha(x) + V(x)$ unchanged. $C_2^Z\, \sigma_{CIS}$ and σ_{TRANS} are identical operations so that $C_2^Z\, \sigma_{CIS}\ \psi_{JKM}\, M(x) = \sigma_{TRANS}\ \psi_{JKM}\, M(x)$ or, $(-1)^K\, \sigma_{CIS}\, M(x) = \sigma_{TRANS}\, M(x)$. This shows that for K even, M(x) has the same cis and trans reflection symmetry, while for K odd, M(x) has opposite cis and

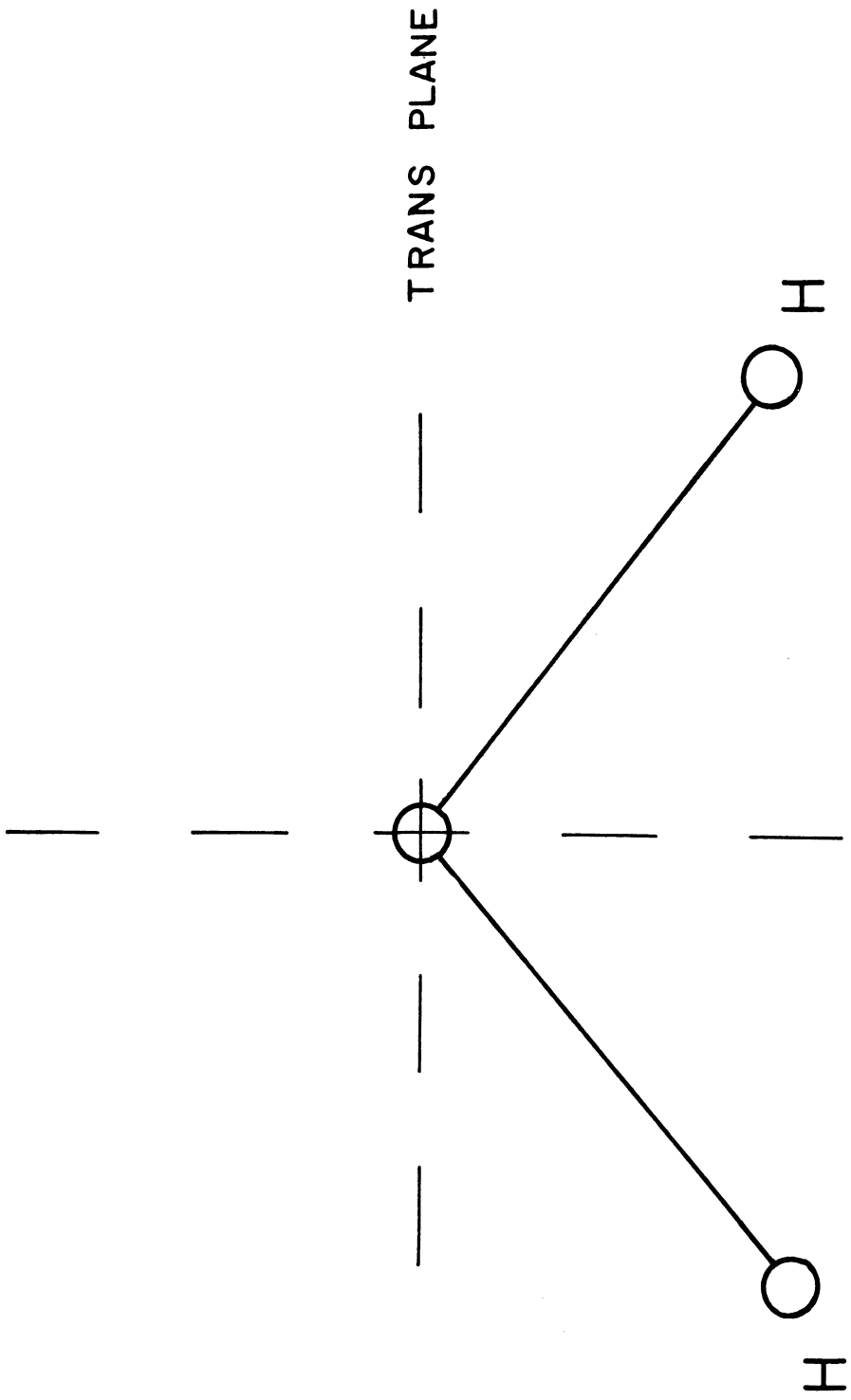

Figure 4. View of H_2O_2 along the O-O bond.

trans reflection symmetry. Thus there are four symmetry species of internal rotation wave functions which can be labeled ea, es, oa, os, where e and o refer to K even or odd, and s and a refer to their trans reflection symmetry. The forms of $M(x) = \sum_{N=-\infty}^{\infty} A_N e^{i(N-K/2)x}$ which have the proper symmetry then are:

$$M_{es}(x) = \sum_{n=0}^{\infty} a_n \cos nx$$

$$M_{ea}(x) = \sum_{n=1}^{\infty} b_n \sin nx$$

$$M_{oa}(x) = \sum_{n=0}^{\infty} c_n \cos(n+1/2)x$$

$$M_{os}(x) = \sum_{n=0}^{\infty} d_n \sin(n+1/2)x$$

The solutions of the internal wave equation depend only on the evenness or oddness of K, not on its magnitude. The four energy matrices for the internal Hamiltonian are then written using these wave functions.

Since levels of opposite inversion symmetry become degenerate for all practical purposes if these levels lie far below the top of the barrier hindering inversion, the levels es and os will have very nearly the same internal energy, as will ea and oa in the case of a high cis barrier. For a high trans barrier, the effectively degenerate pairs of levels will be es, oa and os, ea. When the barriers are

identical, there is no distinction between trans and cis inversion so that the internal eigenvalues os and oa must be degenerate. The ordering of the internal levels in the three cases is shown in Figure 5. It is convenient to label the internal levels by the quantum numbers n and τ such that for each n there are the levels $\tau = 1 = es$, $\tau = 2 = os$, $\tau = 3 = oa$, $\tau = 4 = ea$, with the four lowest energy levels being designated n = 0, the next four n = 1, etc.

$\beta(x)$, $\nu(x)$, and $\gamma(x)$ are symmetric with respect to both cis and trans reflection. $\delta(x)$ is symmetric under trans reflection but antisymmetric under cis reflection. The matrix elements of the total Hamiltonian from the state $n\tau JK_{\pm}$ to the state $n'\tau'J'K'_{\pm}$ which will be denoted by $H^{n'\tau'J'K'_{\pm}}_{n\tau JK_{\pm}}$ are as follows:

$$H^{n\tau JK_+}_{n\tau JK_+} = H^{n\tau JK_-}_{n\tau JK_-} = \beta^{n\tau}_{n\tau} J(J+1) + \nu^{n\tau}_{n\tau} K^2 + W_{n\tau} \quad ; \quad K \neq 1$$

$$H^{n\tau J1_{\pm}}_{n\tau J1_{\pm}} = \left(\beta^{n\tau}_{n\tau} \pm \tfrac{1}{2}\gamma^{n\tau}_{n\tau}\right) J(J+1) + \nu^{n\tau}_{n\tau} + W_{n\tau}$$

$$H^{n'\tau JK_+}_{n\tau JK_+} = H^{n'\tau JK_-}_{n\tau JK_-} = \beta^{n'\tau}_{n\tau} J(J+1) + \nu^{n'\tau}_{n\tau} K^2 \quad ; \quad n' \neq n \,, \; K \neq 1$$

$$H^{n'\tau J1_{\pm}}_{n\tau J1_{\pm}} = \left(\beta^{n'\tau}_{n\tau} \pm \tfrac{1}{2}\gamma^{n'\tau}_{n\tau}\right) J(J+1) + \nu^{n\tau}_{n\tau} \quad ; \quad n' \neq n$$

$$H^{n'\tau J(K\pm2)_+}_{n\tau JK_+} = H^{n'\tau J(K\pm2)_-}_{n\tau JK_-} = \tfrac{1}{2}\gamma^{n'\tau}_{n\tau}\left[(J\mp K)(J\mp K-1)(J\pm K+1)(J\pm K+2)\right]^{1/2}$$

$$H^{n'\tau' J(K\pm1)_+}_{n\tau JK_+} = H^{n'\tau' J(K\pm1)_-}_{n\tau JK_-} = \frac{\mp i(2K\pm1)}{2}\delta^{n'\tau'}_{n\tau}\left[(J\pm K+1)(J\mp K)\right]^{1/2} \quad ; \quad \tau \neq \tau'$$

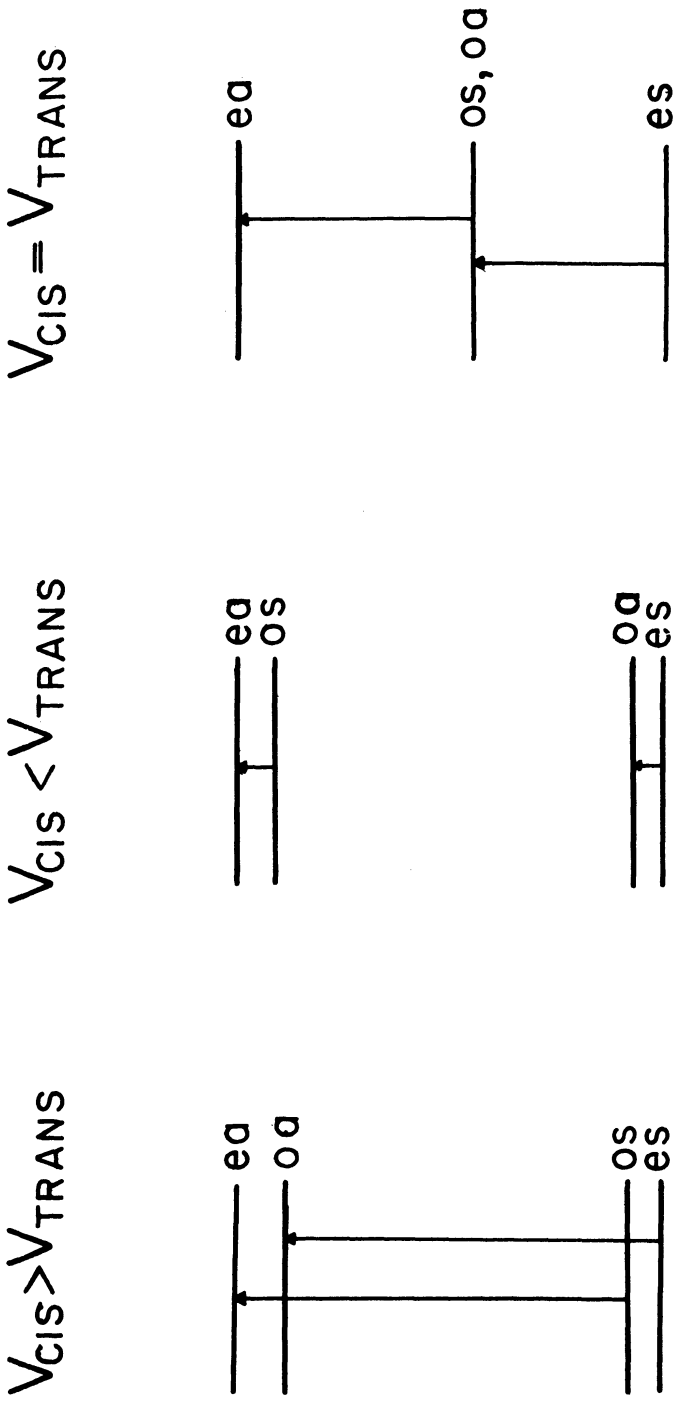

Figure 5. Ordering of internal rotation levels and allowed transitions.

where $\tau',\tau = 2,1$ or $4,3$ and $W_{n\tau}$ are the eigenvalues of the internal Hamiltonian.

For the parameters previously cited, $\delta^{n'\tau'}_{n\tau} < 0.09$ cm^{-1}, $\gamma^{n'\tau}_{n\tau} < 0.037$ cm^{-1}. Further, for $n \neq n'$, $\beta^{n'\tau}_{n\tau} < 0.003$ cm^{-1}, $\nu^{n'\tau}_{n\tau} < 0.10$ cm^{-1}. (This is because $\beta_o{}^{n'\tau}_{n\tau} = \nu_o{}^{n'\tau}_{n\tau} = 0$.) On the other hand, $\nu^{n\tau}_{n\tau}$ is about 9 cm^{-1} and $W_{n\tau}-W_{n'\tau'}$ for $n \neq n'$ will be an order of magnitude larger than this if the hindering of the internal rotation is appreciable (as turns out to be the case). It follows then that

$$\left| H^{n'\tau'JK'_{\pm}}_{n\tau JK_{\pm}} \right| << \left| H^{n\tau JK_{\pm}}_{n\tau JK_{\pm}} - H^{n'\tau'JK'_{\pm}}_{n'\tau'JK'_{\pm}} \right|$$

for $n\tau JK_{\pm} \neq n'\tau'J'K'_{\pm}$ if the J values are restricted to those levels which have an appreciable population. It is a good approximation, therefore, to diagonalize the total energy determinant using second order perturbation theory. The approximate eigenvalues $E_{n\tau JK_{\pm}}$ are then given by the formula:

$$E_{n\tau JK_{\pm}} = H^{n\tau JK_{\pm}}_{n\tau JK_{\pm}} + \sum_{\substack{n'\tau'JK'_{\pm} \\ \neq n\tau JK_{\pm}}} \frac{\left| H^{n'\tau'JK'_{\pm}}_{n\tau JK_{\pm}} \right|^2}{H^{n\tau JK_{\pm}}_{n\tau JK_{\pm}} - H^{n'\tau'JK'_{\pm}}_{n'\tau'JK'_{\pm}}}$$

It should be noted that there is the possibility of near degeneracy of certain levels which are connected by off-diagonal matrix elements in which case this second order approximation will break down. Accidental

degeneracies and second order terms which are of particular significance will be discussed in conjunction with the experimental results.

Since the off-diagonal terms are small, K_+, K_-, τ, n are almost good quantum numbers. To second order and for $K \geq 4$ the distinction between K_+ and K_- disappears and K itself is nearly a good quantum number. The dipole moment is along the C_2 axis of symmetry for all x so that the selection rule for K is $\Delta K = \pm 1$. The J selection rule is, as usual, $\Delta J = 0, \pm 1$. The X axis has been chosen to be the C_2 axis. Since

$$C_2^X \psi_{JK_+M} = \begin{cases} +\psi_{JK_+M} & \text{if J is even} \\ -\psi_{JK_+M} & \text{if J is odd} \end{cases}$$

$$C_2^X \psi_{JK_-M} = \begin{cases} -\psi_{JK_-M} & \text{if J is even} \\ +\psi_{JK_-M} & \text{if J is odd} \end{cases}$$

it follows that the selection rules for $K_\pm$ are:

$$\left.\begin{aligned} K_+ &\leftrightarrow (K\pm1)_+ \\ K_- &\leftrightarrow (K\pm1)_- \end{aligned}\right\} \text{for } \Delta J = 0$$

$$K_+ \leftrightarrow (K\pm1)_- \quad \text{for } \Delta J = \pm 1$$

The dipole moment is invariant under cis reflection but changes sign under trans reflection. Allowed transitions between internal levels are therefore; es $\leftrightarrow$ oa and ea $\leftrightarrow$ os; or in terms of n and τ, n1 $\leftrightarrow$ n'3 and n2 $\leftrightarrow$ n'4. Figure 5 shown these transitions.

Under interchange of the hydrogen atoms, the total wave function must change sign. Rotation by π about the C_2 symmetry axis exchanges

the hydrogen atoms but does not affect $M_{n\tau}(x)$, nor presumably, the electronic wave function. It follows that for even J the K_- levels have nuclear spin weight 3 and the K_+ levels have nuclear spin weight 1 while for odd J the situation is reversed.

Because $\gamma(x)$, $\delta(x)$, and the off-diagonal matrix elements of the Hamiltonian are small and because $\beta(x)$ depends weakly on the internal angle x, it is evident from the above selection rules that if the internal rotational energy is well below the barrier potential, the hindered rotation bands will have features characteristic of an ordinary symmetric top perpendicular band, that is, a pile up of $\Delta J = 0$ transitions to form prominent Q branches averaging $2\nu_{n\tau}^{n\tau}$ or about 18 cm^{-1} in spacing. An exception occurs for the Q branches involving K = 1 which should be spread out due to the J(J+1) dependence of the K = 1 levels on $\gamma_{n\tau}^{n\tau}$, as occurs for any slightly asymmetric top. Figure 6 shows the transitions between the states n and n'. (The levels have been drawn for $V_{CIS} > V_{TRANS}$.) Alternation in the Q branch spacing will occur if the even and odd K internal levels of a given n are not nearly degenerate and if the hindered rotation splittings of the states n and n' are not too similar.

Each Q branch forms the center of a Q sub-band which includes $\Delta J = \pm 1$ transitions. These transitions will give rise to absorption lines on either side of the Q branch spaced about $2\beta_{n\tau}^{n\tau}$ or 1.7 cm^{-1} apart. These lines can be expected to be weak relative to the Q

branches and, in addition, overlapped by similar lines from other sub-bands.

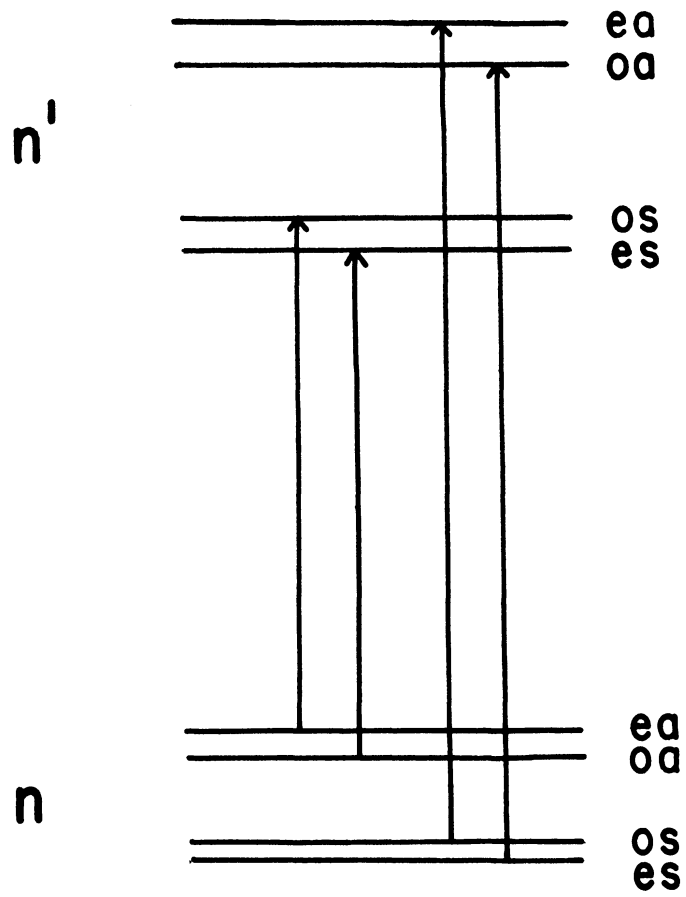

Figure 6. Transitions between the internal rotation states n and n'.

IV. EXPERIMENTAL RESULTS

4.1 PRESENTATION OF THE EXPERIMENTAL DATA

The observed absorption peaks are plotted versus frequency in Figures 7 and 8. Because of the uncertainty as to the H_2O_2 vapor pressure in the absorption cell, the estimated relative intensities of the various lines may be subject to considerable error. The positions of the principal absorption lines are listed in Table II. The percent absorption at the peak and the estimated half-width of the lines are also included in the table.

The gross features of the spectrum can be summarized as:

i. A doubled series of lines below 120 cm^{-1} identified on Figure 7 by A's.

ii. A maze of lines in the 120 to 400 cm^{-1} region.

iii. Several fairly well separated series of lines above 400 cm^{-1}.

iv. A background throughout the spectrum of semi-continuous absorption with some resolved weak structure which incidentally has not been reproduced too faithfully.

In view of the predicted perpendicular character of the hindered rotation bands, the stronger absorptions (i,ii,iii) are presumed to be Q branches ($\Delta J = 0$), while the weaker absorption of iv are similarly presumed to be due to the P and R ($\Delta J = \pm 1$) branches of the sub-bands.

Seven hindered rotation bands have been identified. The frequencies of their band centers are listed in Table III along with the in-

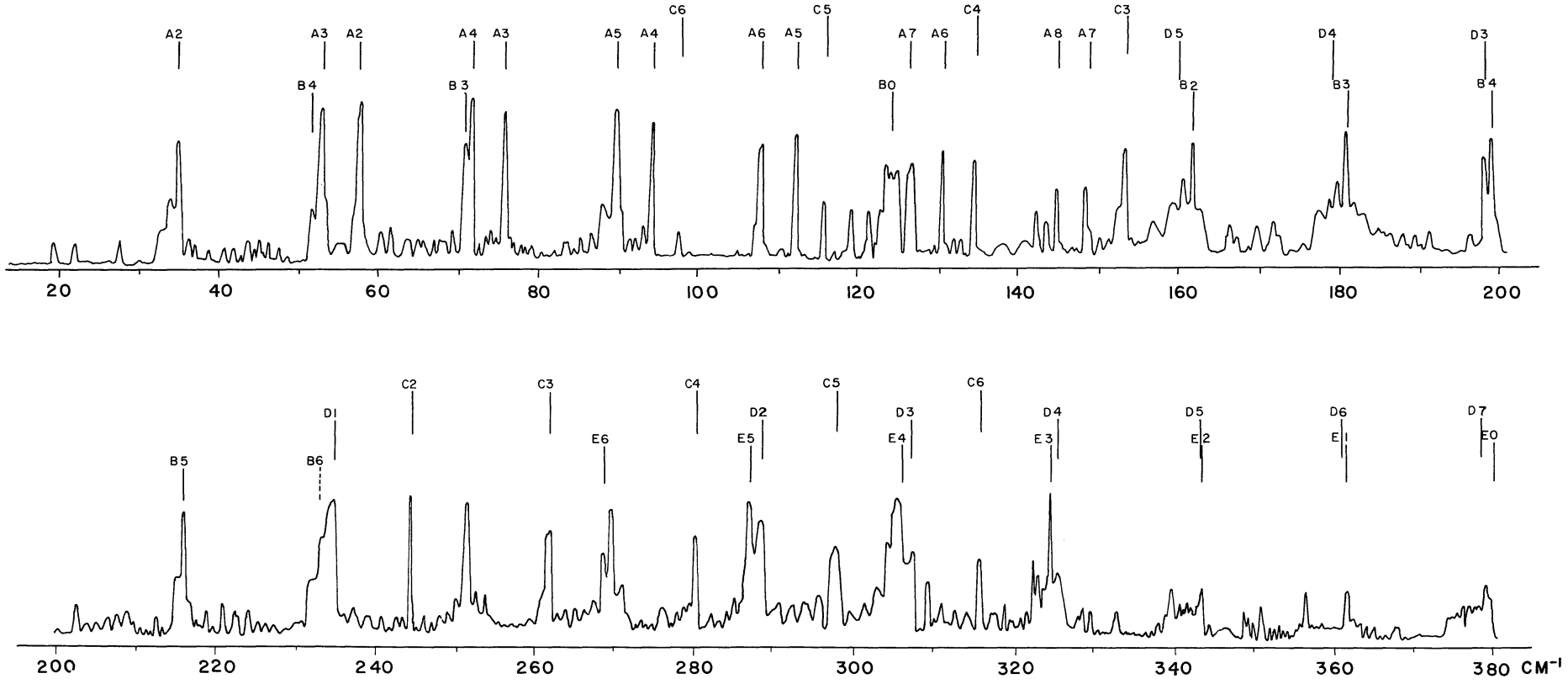

Figure 7. H_2O_2 absorption 15-380 cm^{-1}.

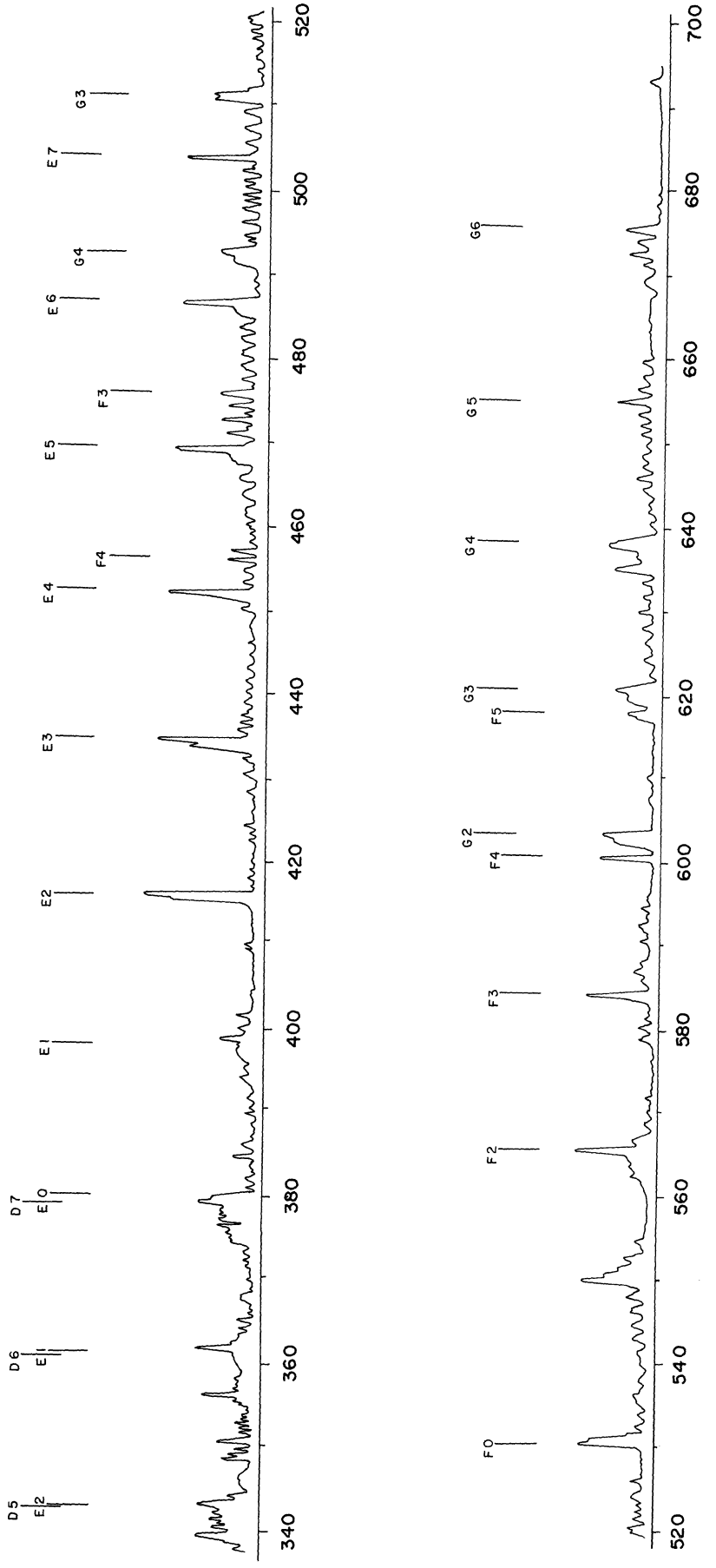

Figure 8. H_2O_2 absorption 340-700 cm^{-1}.

TABLE II

FREQUENCIES OF PRINCIPAL ABSORPTIONS

Sample: 98% H_2O_2 Temperature: ~25°C

Path Length: 1.6 meters 30 to 452 cm^{-1} 4.8 meters 452 to 675 cm^{-1}

Frequency (cm^{-1})	% Absorption	Half-Width (cm^{-1})	Frequency (cm^{-1})	% Absorption	Half-Width (cm^{-1})	Frequency (cm^{-1})	% Absorption	Half-Width (cm^{-1})
34.56	45	0.4	161.98	43	0.6	361.94	27	-
51.78	20	-	179.14	38	0.7	379.44	27	-
52.94	55	0.9	180.11	52	0.7	399.01	20	-
57.38	60	0.5	196.75	35	1.0	416.11	42	1.0
70.49	40	-	197.99	45	1.0	434.06	30	1.3
71.36	62	0.7	215.74	45	0.5	451.70	23	1.0
75.67	50	0.5	234.2	50	1.9	456.21	26	0.6
89.69	55	0.8	244.00	55	0.5	469.20	45	1.2
94.08	45	0.5	251.34	50	1.1	475.40	25	0.7
97.57	15	0.4	261.97	40	1.0	486.61	33	1.2
107.90	38	0.9	267.97	36	0.9	492.5	17	2.0
112.27	42	0.4	269.42	47	1.1	503.85	33	0.8
115.91	24	0.6	279.96	38	0.7	511.3	17	1.9
120.10	20	0.8	286.93	48	1.4	530.4	21	1.3
121.81	20	0.4	288.42	43	1.3	549.4	24	1.2
124.5	30	2.0	297.65	34	1.2	566.41	30	0.7
126.76	30	0.7	305.4	50	2.0	583.80	30	0.7
130.33	40	0.4	307.10	32	0.9	601.01	22	0.7
134.37	35	0.5	308.96	20	0.5	603.0	20	1.6
142.19	20	0.4	315.42	30	0.9	617.8	12	0.9
143.42	17	0.6	322.44	30	-	620.6	17	2.0
144.55	28	0.5	324.46	52	0.6	634.9	14	0.7
148.37	26	0.7	339.77	23	-	638.3	17	0.9
152.92	40	0.6	343.31	25	-	655.5	12	0.9
160.71	31	0.8	357.27	26	-	674.5	12	0.6

ternal level assignments for the transition. The letter designation of each band corresponds to the letter identification of the Q branch series of each band shown in Figures 7 and 8. The number designation on the Q branch series in Figures 7 and 8 gives the K value of the initial state.

TABLE III

OBSERVED BAND FREQUENCIES AND BAND ASSIGNMENTS

Band	Frequency (cm^{-1})	Transition $n\tau \rightarrow n'\tau'$
(A)	11.43	01 ⟷ 03 and 02 ⟷ 04
(B)	116.51	11 → 13 and 12 → 14
(C)	198.57	13 → 21 and 14 → 22
(D)	242.76	03 → 11 and 04 → 12
(E)	370.70	01 → 13 and 02 → 14
(F)	521.68	11 → 2,3 and 12 → 24
(G)	557.84	03 → 2,1 and 04 → 22

These seven series account for nearly all of the stronger absorption lines of the spectrum. The justification for these assignments is presented in detail in a later section of this chapter.

No alternation in Q branch spacings of a particular series is observed. This indicates a relatively high cis barrier with negligible tunneling through it.

The hindering potential V(x) required to fit these internal transitions is dependent, of course, on the bond parameters chosen. It is necessary to fit both the observed internal levels and the observed

matrix elements of $\beta(x)$, $\nu(x)$, $\gamma(x)$, $\delta(x)$, (which determine the structure of the bands) with the four quantities $V(x)$, r_{00}, r_{0H}, and the 0-0-H angle. From analysis of the present bands and re-interpretation of the near infrared and microwave data in light of the present theory, the most accurately known matrix elements are thought to be; $\beta_{01}^{01} = 0.8564 \pm .001$ cm^{-1}, $\gamma_{01}^{01} = -0.017 \pm .001$ cm^{-1}, and $\nu_{01}^{01} = 9.209 \pm .005$ cm^{-1}. These matrix elements appear in the first order expressions for the energy of the ground internal state.

$$H^{01\,J\,K_\pm}_{01\,J\,K_\pm} = \beta_{01}^{01}\, J(J+1) + V_{01}^{01}\, K^2 + W_{01} \quad ; \quad K \neq 1$$

$$H^{01\,J\,1_\pm}_{01\,J\,1_\pm} = \left(\beta_{01}^{01} \pm \tfrac{1}{2}\gamma_{01}^{01}\right) J(J+1) + V_{01}^{01} + W_{01}$$

The determination of their values will be discussed later.

Diagonalization of the internal energy matrix, computation of the internal wavefunction $M_{n\tau}(x)$, and evaluation of the matrix elements involving these wave functions were carried out on an IBM 709 computer using a program written by Leacock for an 18 by 18 matrix. Figure 9 compares the observed internal levels with those calculated from the hindering potential $V(x) = 993 \cos x + 636 \cos 2x + 44 \cos 3x$, $r_{00} = 1.475$ A$^\circ$, $r_{0H} = 0.950$ A$^\circ$, and an 0-0-H angle of 94.8°. It is seen that this three term potential is sufficient to fit the five experimental level positions quite well. In addition, these four quantities yield $\beta_{01}^{01} = 0.8574$ cm^{-1}, $\gamma_{01}^{01} = -0.0168$ cm^{-1}, and $\nu_{01}^{01} = 9.205$ cm^{-1} which are within the experimental errors for these matrix elements.

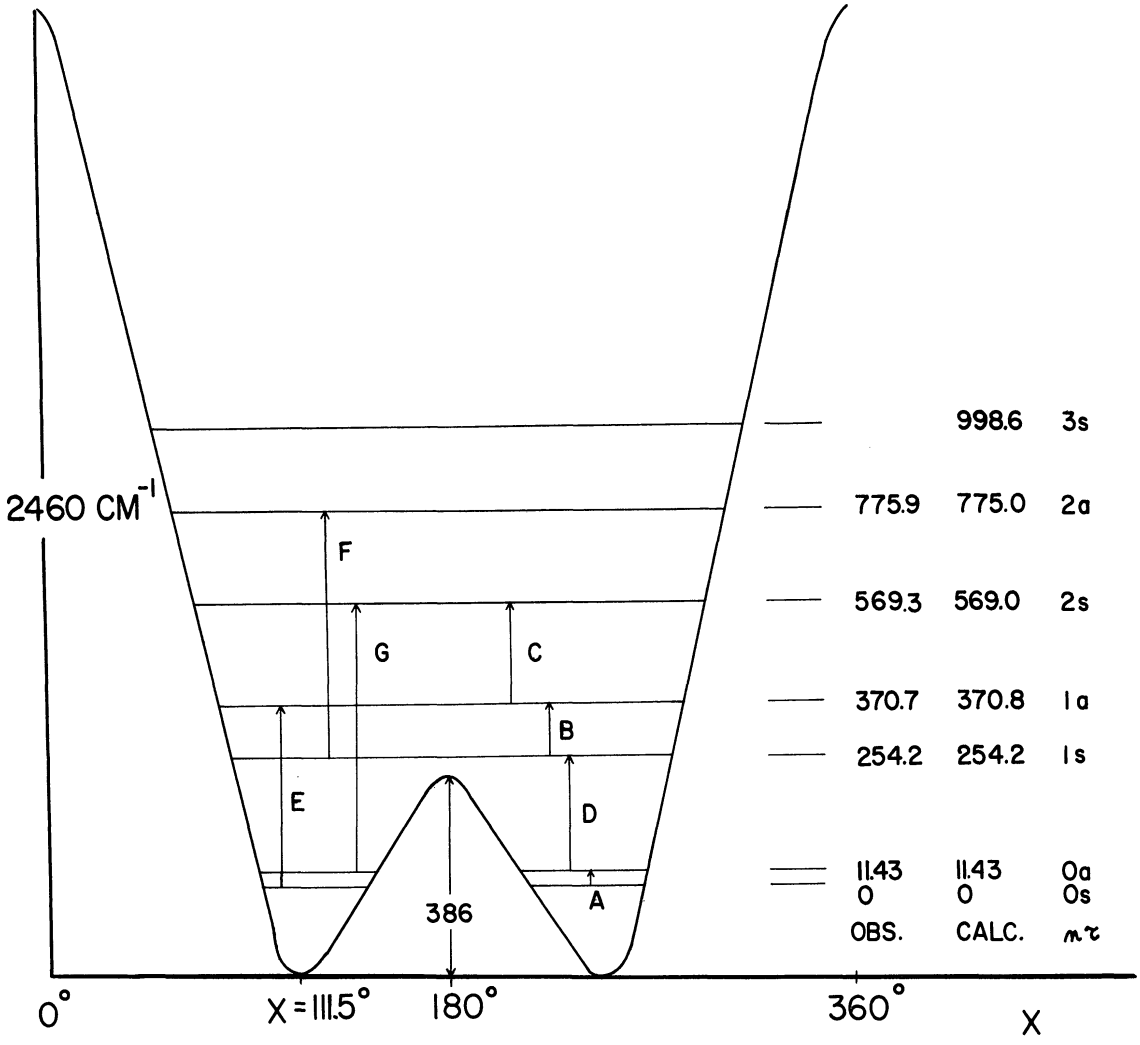

Figure 9. Internal rotation level structure of H_2O_2.

The main features of this hindering potential are: a cis barrier of 2460 cm^{-1}, a trans barrier of 386 cm^{-1}, and a potential minimum 111.5^{o} from the cis configuration. Both of these barriers are considerably smaller than those predicted by Penney and Sutherland (1). In particular, the trans barrier is an order of magnitude lower.

The levels n1 and n2 for $n \leq 2$ are computed to be separated by less than 0.01 cm^{-1} as are the levels n3 and n4. This is a consequence of negligible tunneling through the cis barrier and results in the internal eigenvalues of interest being effectively independent of the K quantum number. Therefore, it is sufficient to label the internal levels by the quantum number n and their trans symmetry s or a as has been done in Figure 9. The allowed internal transitions are then ns $\leftrightarrow$ n'a. The seven observed transitions are lettered in Figure 9 to correspond to the lettering of Table III. The position of the lowest energy internal level, it might be noted, is computed to be 170.04 cm^{-1} above the potential energy minimum.

Table IV lists the largest x dependent matrix elements of the various types occuring in the off-diagonal elements of the total Hamiltonian. Since the smallest difference in internal levels of different n ($\tau \neq \tau'$) is $W_{11} - W_{01} = 254.2$ cm^{-1}, most second order corrections to the energy levels are negligibly small. Leacock (15) has written out the leading terms in the energy level formulae. His results are:

$$E_{n\tau J0} \cong J(J+1)\left[\beta_{n\tau} - \frac{\tfrac{1}{2}\,|\delta_{n\tau}^{n\tau'}|^2}{\tfrac{1}{2}J(J+1)\gamma_{n\tau} + \nu_{n\tau}}\right] + W_{n\tau}$$

$$+ J^2(J+1)^2\left[-\frac{|\gamma_{n\tau}|^2}{8\nu_{n\tau}} + \tfrac{1}{2}\sum_{n'=n\pm1} \frac{|\gamma_{n\tau}^{n'\tau}|^2}{W_{n\tau} - W_{n'\tau} - 4\nu_{n\tau}}\right]$$

$$E_{n\tau J1_+} \cong J(J+1)\left[\beta_{n\tau} + \tfrac{1}{2}\gamma_{n\tau} - \tfrac{3}{4}\,\frac{|\delta_{n\tau}^{n\tau'}|^2}{\nu_{n\tau}} + \tfrac{1}{2}\,\frac{|\delta_{n\tau}^{n\tau'}|^2}{\tfrac{1}{2}J(J+1)\gamma_{n\tau} + \nu_{n\tau}}\right]$$

$$+ J^2(J+1)^2\left[-\frac{|\gamma_{n\tau}|^2}{32\nu_{n\tau}} + \tfrac{1}{4}\sum_{n'=n\pm1}\left\{\frac{|\gamma_{n\tau}^{n'\tau}|^2}{W_{n\tau} - W_{n'\tau}} + \frac{|\gamma_{n\tau}^{n'\tau}|^2}{W_{n\tau} - W_{n'\tau} - 8\nu_{n\tau}}\right\}\right]$$

$$+ \nu_{n\tau} + W_{n\tau}$$

$$E_{n\tau J1_-} \cong J(J+1)\left[\beta_{n\tau} - \tfrac{1}{2}\gamma_{n\tau} - \tfrac{3}{4}\,\frac{|\delta_{n\tau}^{n\tau'}|^2}{\nu_{n\tau}}\right] + \nu_{n\tau} + W_{n\tau}$$

$$+ J^2(J+1)^2\left[-\frac{|\gamma_{n\tau}|^2}{32\nu_{n\tau}} + \tfrac{1}{4}\sum_{n'=n\pm1}\left\{\frac{|\gamma_{n\tau}^{n'\tau}|^2}{W_{n\tau} - W_{n'\tau}} + \frac{|\gamma_{n\tau}^{n'\tau}|^2}{W_{n\tau} - W_{n'\tau} - 8\nu_{n\tau}}\right\}\right]$$

$$E_{n\tau J2_+} \cong J(J+1)\left[\beta_{n\tau} - \tfrac{1}{2}\,\frac{|\delta_{n\tau}^{n\tau'}|^2}{\nu_{n\tau}}\right] + 4\nu_{n\tau} + W_{n\tau}$$

$$+ J^2(J+1)^2\left[\frac{5}{48}\,\frac{|\gamma_{n\tau}|^2}{\nu_{n\tau}} + \tfrac{1}{2}\sum_{n'=n\pm1}\left\{\frac{|\gamma_{n\tau}^{n'\tau}|^2}{W_{n\tau} - W_{n'\tau} + 4\nu_{n\tau}} + \frac{\tfrac{1}{2}\,|\gamma_{n\tau}^{n'\tau}|^2}{W_{n\tau} - W_{n'\tau} - 16\nu_{n\tau}}\right\}\right]$$

$$E_{n\tau J2_-} \cong J(J+1)\left[\mathcal{B}_{n\tau} - \tfrac{1}{2}\,\frac{|\delta_{n\tau}^{n\tau'}|^2}{\nu_{n\tau}}\right] + 4\nu_{n\tau} + W_{n\tau}$$

$$+ J^2(J+1)^2\left[-\frac{|\gamma_{n\tau}|^2}{48\nu_{n\tau}} + \tfrac{1}{4}\sum_{n'=n\pm1}\frac{|\gamma_{n\tau}^{n'\tau}|^2}{W_{n\tau}-W_{n'\tau}-12\nu_{n\tau}}\right]$$

For $K \geqq 3$

$$E_{n\tau JK_\pm} \cong J(J+1)\left[\mathcal{B}_{n\tau} - \tfrac{1}{2}\,\frac{|\delta_{n\tau}^{n\tau'}|^2}{\nu_{n\tau}}\right] + K^2\nu_{n\tau} + W_{n\tau}$$

$$+ J^2(J+1)^2\left[\frac{1}{8(K^2-1)}\,\frac{|\gamma_{n\tau}|^2}{\nu_{n\tau}} + \tfrac{1}{2}\sum_{n'=n\pm1}\frac{|\gamma_{n\tau}^{n'\tau}|^2\left(W_{n\tau}-W_{n'\tau}-4\nu_{n\tau}\right)}{\left[W_{n\tau}-W_{n'\tau}-4\nu_{n\tau}\right]^2-\left[4K\nu_{n\tau}\right]^2}\right]$$

TABLE IV

LARGEST SECOND ORDER MATRIX ELEMENTS

Matrix Elements	Squared Value
δ_{12}^{12}	0.0047
δ_{21}^{32}	0.0004
γ_{11}^{11}	0.0005
γ_{01}^{11}	0.0005
β_{01}^{11}	0.00001
ν_{01}^{11}	0.0048

where $\tau' = 2$ if $\tau = 1$, $\tau' = 4$ if $\tau = 3$ and conversely. The superscripts have been dropped from matrix elements diagonal in both n and τ. Here asymmetry connections $\gamma_{n\tau}^{n'\tau}$ between states for which $|n'-n| > 1$ have been neglected because of the large energy denominators involved.

The matrix elements required to compute the energy levels through n = 2 are given in Table V.

TABLE V

CALCULATED MATRIX ELEMENTS

(cm^{-1})

$n\tau$	$\beta_{n\tau}$	$\nu_{n\tau}$	$\gamma_{n\tau}$
0s	.8574	9.204	-.0168
0a	.8574	9.198	-.0148
1s	.8575	9.226	-.0228
1a	.8576	9.199	-.0148
2s	.8578	9.196	-.0136
2a	.8580	9.186	-.0100

$\delta_{01}^{02} = -.058$	$\gamma_{01}^{11} = -.010$	$\gamma_{13}^{24} = .013$
$\delta_{03}^{04} = -.055$	$\gamma_{02}^{12} = .010$	$\gamma_{14}^{24} = .013$
$\delta_{11}^{12} = -.069$	$\gamma_{03}^{13} = .010$	$\gamma_{21}^{31} = -.014$
$\delta_{13}^{14} = -.056$	$\gamma_{04}^{14} = .010$	$\gamma_{22}^{32} = .014$
$\delta_{21}^{22} = -.055$	$\gamma_{11}^{21} = -.012$	$\gamma_{23}^{33} = .015$
$\delta_{23}^{24} = -.050$	$\gamma_{12}^{22} = -.012$	$\gamma_{24}^{34} = -.015$

When no distinction between $\tau = 1$ and $\tau = 2$ or between $\tau = 3$ and $\tau = 4$ is necessary, the s, a, labeling will generally be used with s for $\tau = 1$ or 2 and a for $\tau = 3$ or 4.

Since $\gamma_{n\tau}$ is negative the levels $n\tau Jo$ and $n\tau' Jl_+$ become resonant through the connection $\delta_{n\tau}^{n\tau'}$ for J values in the neighborhood of 30. However, calculations based on symmetric top intensity factors indicate that the transitions which involve $J > 25$ are of such low intensity that their contribution to the spectrum can be ignored. For $J < 25$, the terms involving $\delta_{n\tau}^{n\tau'}$ contribute only a few parts in 10^4 to the coefficient of $J(J+1)$ which, considering the accuracy of the experimental data presently available, turns out to be almost negligible. The energy level formulae therefore, are very nearly what would be obtained from a second order perturbation treatment of a slightly asymmetric top having closely spaced vibrational levels with $\beta_{n\tau}$, $\nu_{n\tau}$, and $\gamma_{n\tau}$ playing the role of the conventional principal axis rotational constants $(B+C)/2$, $A-(B+C)/2$ and $(B-C)/2$, respectively.

In most instances the contribution by the elements off diagonal in n is small, but in a few cases of interest the energy levels $n\tau JK$ and $n'\tau JK+2$ turn out to be nearly degenerate and are quite strongly affected by the asymmetry connection $\gamma_{n\tau}^{n'\tau}$. These cases will be discussed in the band analysis section.

4.2 ANALYSIS AND DISCUSSION OF THE BANDS

The fine structure of each of the bands reported in the previous

chapter should have the appearance of a perpendicular type vibration-rotation band, that is, a set of regularly spaced intense Q lines fairly far apart (about 18 cm^{-1}) with relatively weak P and R branch lines accompanying each of these Q lines. The separation of the P and R lines is determined primarily by the value of β_{nT} and should be of the order of 1.7 cm^{-1}. At room temperature, the maximum of the Boltzmann distribution occurs for J = 10. Consequently, the P and R lines will spread over tens of cm^{-1} and the P and R lines of one sub-band will intermingle with those of adjacent sub-bands. It was estimated that an order of magnitude increase in resolution of our spectrometer would be necessary to analyze the P and R branches under these circumstances. Fortunately, the frequencies and contours of the Q lines suffice to give a great deal of information about the internal motion of the molecule.

For $K \geq 3$, the predicted Q branch widths are narrower than the spectrograph's band pass except for several cases of near resonance. The predicted widths of R_{Q_2} and P_{Q_3} are slightly greater than the spectral slit width. As a result all but the Q branches involving K = 1 should fit an ordinary symmetric top perpendicular band analysis with centrifugal distortion terms included. In most bands such an analysis enables one to identify the Q branches. However, in those bands which turn out to have only a few identifiable Q branches, the calculated shape of the Q branches involving K = 1 is very helpful in making the assignments.

For purposes of analysis the peak absorption frequencies of the Q branches are taken as approximate Q sub-band heads. In the symmetric top approximation the frequencies of the Q sub-band heads in the $n\tau \rightarrow n'\tau'$ hindered rotation band are:

$$R_{Q_K}(0) = \nu_{n'\tau'}(K+1)^2 - \nu_{n\tau}K^2 + W_{n'\tau'} - W_{n\tau} - D_K[(K+1)^4 - K^4]$$

$$P_{Q_K}(0) = \nu_{n'\tau'}(K-1)^2 - \nu_{n\tau}K^2 + W_{n'\tau'} - W_{n\tau} - D_K[(K-1)^4 - K^4]$$

where a distortion coefficient D_K has been added to correct for vibration-rotation interactions.

Figures 7 and 8 show the Q branch assignments for the various bands. The numbers refer to the initial K value in the transition. The two series of Q branches labeled A beginning near the low frequency end of the spectrum and extending to about 150 cm^{-1} with decreasing intensity arise from the internal transitions Os → Oa and Oa → Os. The absence of any other strong series of Q branches beginning at low frequency is evidence that there are no lower energy hindered rotation states with a consequent smaller splitting. These series were analyzed using the combination sum relations:

$$\frac{Q_{K-1,\,s\rightarrow a} + Q_{K,\,a\rightarrow s}}{4K} = \nu_{Os} - 2(K^2+1)D_K$$

$$\frac{Q_{K-1,\,a\rightarrow s} + Q_{K,\,s\rightarrow a}}{4K} = \nu_{Oa} - 2(K^2+1)D_K$$

Figure 10 shows what are felt to be the most reliable combination sums plotted versus K^2. The error flags represent an estimated error of 0.1 cm^{-1} in the combination sums. The lines to be drawn are somewhat ambiguous. If it is required that their slopes $-2D_K$ be the same, then lines which yield $D_K = 4.4 \times 10^{-4}$ cm^{-1}, $\nu_{0s} = 9.209$ cm^{-1}, and $\nu_{0a} = 9.203$ cm^{-1} are reasonable. Such a choice agrees with the theoretically predicted difference $\nu_{0s} - \nu_{0a} = +0.006$ cm^{-1} (see Table V) but it should be noted that the errors are of similar magnitude.

Table VI shows observed Q branch frequencies and those calculated using the band constants above and a ground state splitting $W_{0a} - W_{0s} = 11.43$ cm^{-1}. (This splitting has been chosen for the most accurate fit to the microwave data which will be discussed later).

TABLE VI

Q BRANCH FREQUENCIES OF THE 0s → 0a AND 0a → 0s TRANSITIONS (cm^{-1})

K	0s → 0a		0a → 0s	
	Calc	Obs	Calc	Obs
0 → 1	20.63	--	- 2.23	- 2.23*
1 → 2	39.03	--	16.17	--
2 → 3	57.39	57.38	34.61	34.56
3 → 4	75.71	75.67	53.00	52.94
4 → 5	94.00	94.08	71.38	71.36
5 → 6	112.20	112.27	89.71	89.69
6 → 7	130.31	130.33	107.96	107.90
7 → 8	148.42	148.37	126.24	126.76
8 → 9	166.42	--	144.41	144.55

*Based on microwave data of Massey and Bianco

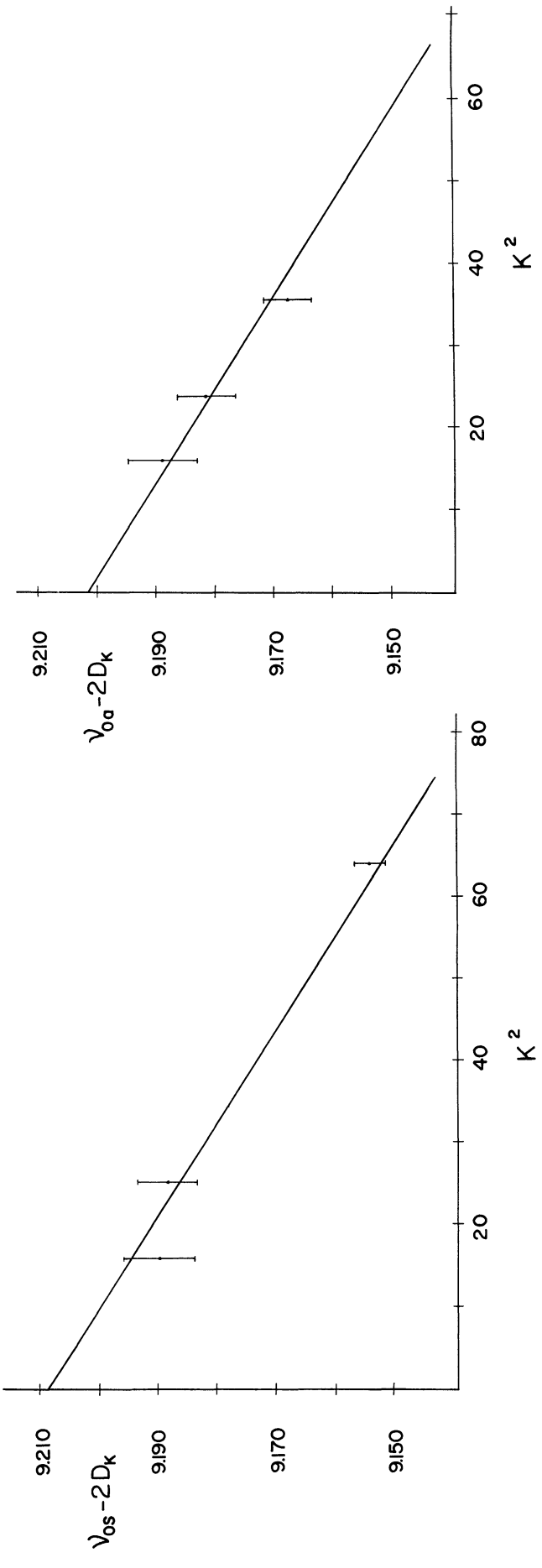

Figure 10. Combination sums for the 11.43 cm^{-1} band.

The only significant disagreement between calculated and observed frequencies occurs for $Q_{7,a \rightarrow s}$. The reason for this seems to be one of the resonance possibilities mentioned earlier. The OsJ8 level would lie about 3.2 cm^{-1} above the 1sJ6 level (based on an experimental value of 9.18 cm^{-1} for ν_{1s}) except that the interaction of these two levels through $\gamma_{n\tau}^{n'\tau}$ $(P_X^2-P_Y^2)$ causes them to be pushed apart. The second order perturbation formulae are not generally valid for these two levels and the levels have been computed by diagonalization of the 2x2 sub-matrix containing the level interaction. The resulting formula for Q_7 is; $Q_7 \cong 126.24-1.34+[7.3+10^{-4}J^2(J+1)^2]^{1/2}$ where 126.24 cm^{-1} is the band head position listed in Table VI. The computed positions and intensities of the components of this Q branch have been plotted in Figure 11 along with the observed absorption. The numbers on the components refer to the J value. The effect of this resonance is seen to be a shift in the Q branch position toward higher frequency in agreement with the observed displacement, although a somewhat greater width is predicted than is observed. However, reference to the Q branch widths shows that in general Q branches of the Os → Oa transition are significantly narrower than Q branches of the Oa → Os transition which tend to exhibit tailing on the low frequency side. This would seem to indicate that there are J dependent terms in the energy levels arising from vibration-rotation interactions which partially cancel the resonance broadening.

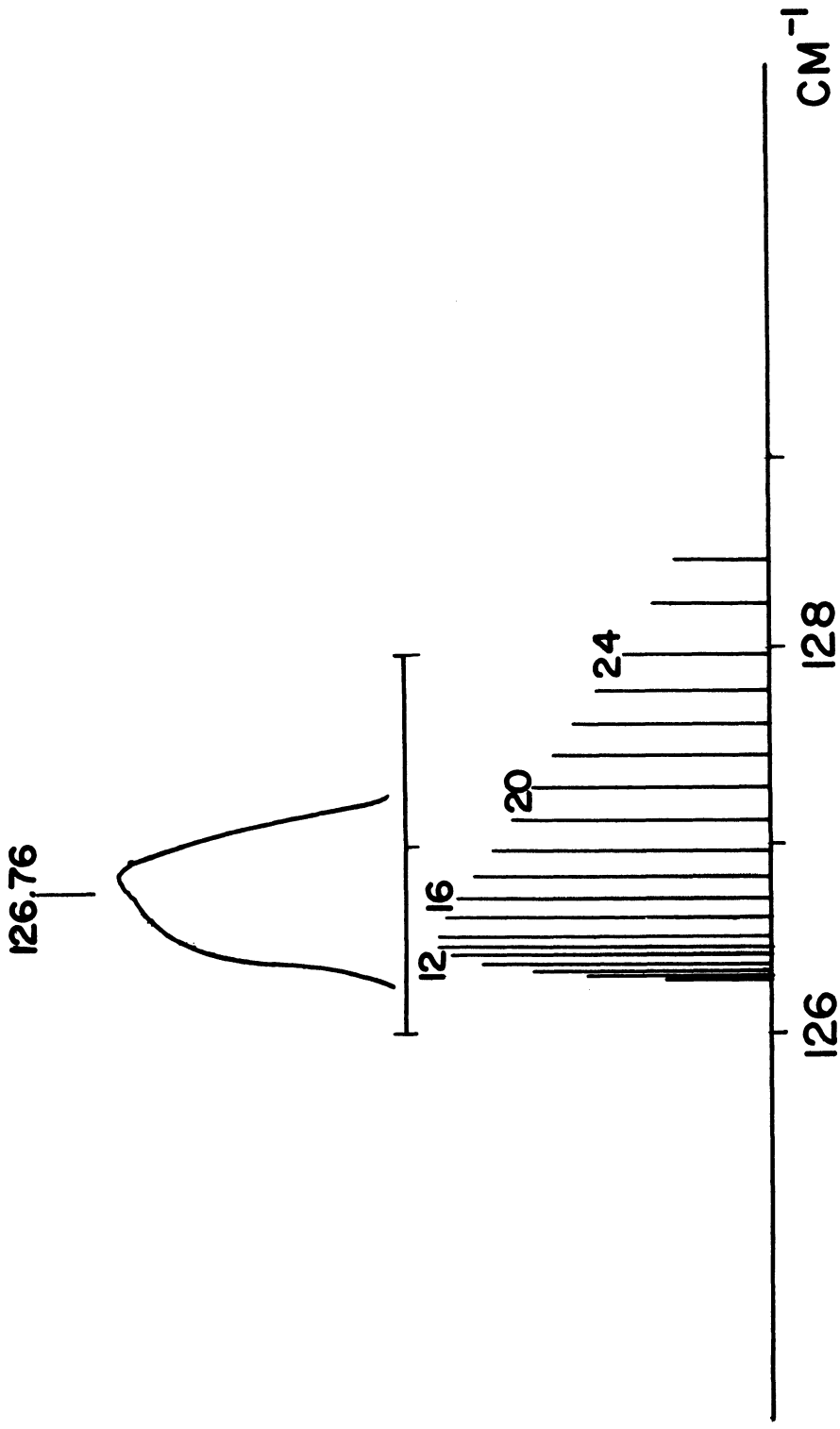

Figure 11. Computed and observed Q_7 branch of the Oa → Os transition.

The spectra showed little or no trace of absorption by Q branches involving K = 1 for this band. Calculations based on the matrix elements listed in Table V show that these Q branches should be several wave-numbers wide and consequently weak.

The remaining bands have been analyzed in a similar fashion using combination differences wherever possible. Table VII lists the band constants so determined including the band discussed above.

TABLE VII

BAND CONSTANTS

(cm^{-1})

Transition		Band	$\nu_{n\tau}$	$\nu_{n\tau}$
$n\tau$	$n'\tau'$	Center	Lower State	Upper State
0s	0a	11.43	9.209	9.203
0s	1a	370.70	9.209	9.139
0a	1s	242.76	9.2	9.2
0a	2s	557.84	9.20	9.11
1s	1a	116.51	9.183	9.142
1s	2a	521.68	9.18	9.05
1a	2s	198.57	9.144	9.113

$D_K = 4.4 \times 10^{-4}$ for all bands.

The average $\nu_{n\tau}$ for each level is listed in Table VIII along with its estimated error.

TABLE VIII

EXPERIMENTAL $\nu_{n\tau}$ VALUES

(cm^{-1})

$\nu_{0s} = 9.209 \pm .005$

$\nu_{0a} = 9.203 \pm .005$

$\nu_{1s} = 9.18 \pm .01$

$\nu_{1a} = 9.142 \pm .005$

$\nu_{2s} = 9.11 \pm .01$

$\nu_{2a} = 9.05 \pm .01$

Taking into consideration that the same level is involved in general in more than one band, the band centers are estimated to be accurate to ±.05 cm^{-1} except for the 11.43 cm^{-1} band which can be determined to ±.01 cm^{-1} from the microwave data.

Table IX lists the observed and computed Q branch frequencies for the remaining six hindered rotation bands. The computed positions are based upon the band centers of Table VII and the rotational constants of Table VIII. Owing to the Q branch widths involved deviations of less than 0.2 cm^{-1} can not be considered significant.

In the following discussion, all calculations of the shapes of the Q branches involving K = 1 are based on the computed matrix elements of Table V.

The 198.57 cm^{-1} band is the least overlapped. There is some unexplained alternation in the Q branch widths on the R side of the band, but otherwise this band is well behaved. Calculations show that the four central Q branches should be sufficiently spread so as to be lost in the background.

The 370.70 cm^{-1} band has a clean R side but several of the P_Q branches are overlapped, especially P_{Q_4} whose identification is uncertain. Spectra taken at 3.2 meters path length show broad absorptions for the four central Q branches. After allowance for the calculated shapes of these Q branches, there seems to be additional broad absorption present shading their low frequency sides. A plot of the P

TABLE IX

OBSERVED AND COMPUTED Q BRANCH POSITIONS FOR SIX HINDERED ROTATION BANDS

Q	ν_0 = 370.70		ν = 198.57		ν = 116.51		ν = 521.68		ν = 557.84		ν = 242.76	
Branch	Calc	Obs	Calc	Obs	Calc	Obs	Calc	Obs	Calc	Obs	Calc	Obs
R_{Q_7}	503.80	503.85										
R_{Q_6}	486.64	486.61	315.47	315.42								
R_{Q_5}	469.30	469.20	297.77	297.65	215.78	215.74	617.94	617.80	655.54	655.5	342.94	**
R_{Q_4}	451.75	451.70	279.95	279.96	197.99	197.98	600.89	601.01	638.26	638.3	324.90	**
R_{Q_3}	434.01	434.06	261.99	261.97	180.06	180.11	583.83	583.80	620.74	620.6	306.76	**
R_{Q_2}	416.11	416.11	243.98	244.00	162.03	161.98	566.41	566.41	603.01	603.0	288.55	288.42
.												
.												
.												
P_{Q_3}	324.42	324.46	152.76	152.92	70.47	70.49	475.28	475.40	511.50	511.3	196.75	196.75
P_{Q_4}	305.77	*	134.38	134.37	51.96	51.78	456.34	456.21	492.69	492.5	178.26	**
P_{Q_5}	286.91	286.93	115.97	115.91							159.80	**
P_{Q_6}	268.02	267.97	97.55	97.57								

*Obscured by other bands.

**Q branches several cm^{-1} wide.

and R structure of these Q sub-bands failed to disclose any accidental piling up. These additional broad absorptions are thought to arise from the 242.76 cm^{-1} band.

By itself the 242.76 cm^{-1} band assignment might be subject to some skepticism. As Table IX shows, R_{Q_2} and P_{Q_3} can be identified and they have about the predicted width, but the Q branches for larger K values all seem to be several cm^{-1} wide, a result not predicted by theory. The computed positions of the Q branches of this band are shown in Figures 7 and 8 to illustrate the broad absorptions which occur at the positions of the higher K Q branches. The frequency assignment of the band center has been made using the level positions determined from the other bands. Calculation of the shapes of the four central Q branches yields an interesting result for P_{Q_1}. Examination of the matrix elements in Table V shows that the 1s level (which is the upper level for the 242.76 cm^{-1} transition) has an unusually large γ_{nT} or "asymmetry" compared to all other levels. β_{nT}, however, is predicted to be very nearly the same for all levels. As a result the second order asymmetry correction to the K = 0 level in the 1s state is of sufficient magnitude to produce significant opposition to the ordinarily large first order $-1/2\ \gamma\ J(J+1)$ spread of the P_{Q_1} branch. The calculated J dependence of this branch is; $P_{Q_1}(J) = 233.56 + 7.2\times10^{-3}\ J(J+1) - 6.1\times10^{-6}\ J^2(J+1)^2$. This is plotted in Figure 12 along with the observed absorption in this region. (Only transitions with nu-

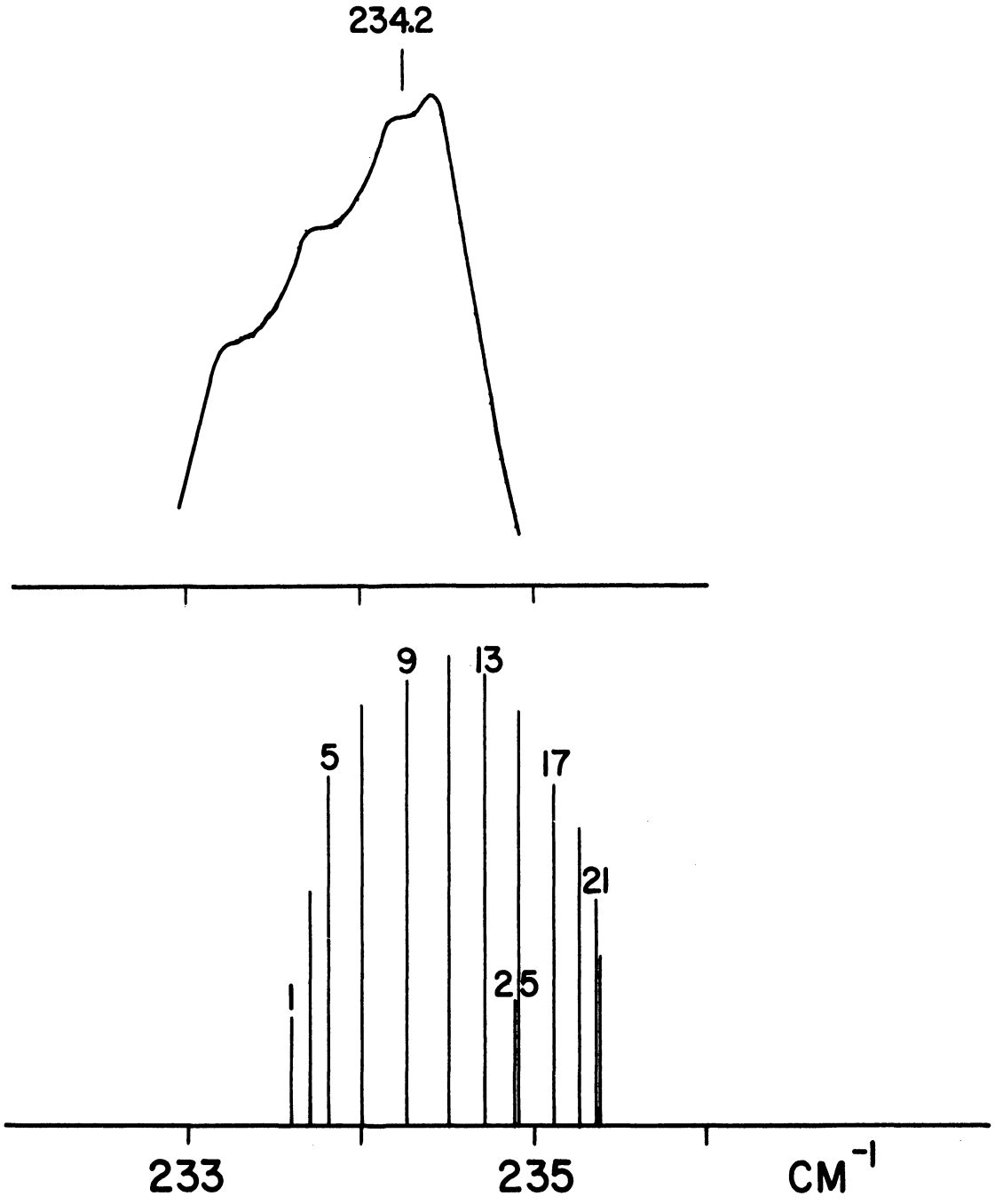

Figure 12. Computed and observed P_{Q_1} branch of the 242.76 cm^{-1} band.

clear spin weight 3 are shown). The computed and observed absorptions are seen to agree well enough in width and position so that there is little doubt the observed absorption is due to P_{Q_1}. This agreement along with the apparently well behaved P_{Q_3} and R_{Q_2} branches would seem to indicate that only the higher K Q branches in this band deviate markedly from theory.

Although the appearance of the P_{Q_1} branch of the 242.76 cm^{-1} band is quite satisfying both in the agreement with the theory and in the fact that an otherwise puzzling absorption is accounted for, the strongest proof for the assignment of that band comes from the identification of the 116.51 cm^{-1} band. Since the same ls level is involved in this band as in the 242.76 cm^{-1} band, it is surprising that four relatively narrow R_Q branches can be identified. Only two P_Q branches are identifiable. This band, like the other bands but to a greater extent, suffers from a rapid decrease in the P_Q branch intensities as K increases because of the frequency factor $h\nu(1-e^{-h\nu/kT})$ in the absorption coefficient. (ν here refers to the frequency of the absorption). Table X gives the calculated relative intensities of the Q branches of this band. The fact that R_{Q_6} can not be readily identified is probably a consequence of the perturbation of the lsJ6 level by the resonance previously discussed. This would tend to shift R_{Q_6} from its normally expected position of 233.43 cm^{-1} and cause it to merge with the broad absorption centered at 234.2 cm^{-1}.

TABLE X

RELATIVE INTENSITIES OF THE Q BRANCHES OF THE 116.51 CM^{-1} BAND

R_{Q_8}	.15	R_{Q_1}	1.29
R_{Q_7}	.31	R_{Q_0}	1.12
R_{Q_6}	.54	P_{Q_1}	.86
R_{Q_5}	.82	P_{Q_2}	.52
R_{Q_4}	1.10	P_{Q_3}	.27
R_{Q_3}	1.34	P_{Q_4}	.11
R_{Q_2}	1.44		

The high asymmetry of the 1s level also produces a narrowing of one of the central Q branches in the 116.51 cm^{-1} band. The computed J dependence of R_{Q_0} of this band is; $R_{Q_0}(J) = 125.67-7.2\times10^{-3}\ J(J+1)+ 6.2\times10^{-6}\ J^2(J+1)^2$. Much of the absorption in the 123-125 cm^{-1} region is probably due to R_{Q_0} as the former has approximately the predicted width and position.

The fact that there are no strong absorptions in the near vicinity of 143 cm^{-1}, 106 cm^{-1}, and 88 cm^{-1} that are otherwise not accounted for supports the 116.51 cm^{-1} band assignment and also, therefore, the 242.76 band assignment.

The 557.84 cm^{-1} band is of interest mainly because it verifies that the 198.57 cm^{-1} band arises from the transition 1a → 2s. It is

characterized by fairly broad Q branches (1 to 2 cm^{-1} in halfwidth) of quite low intensity.

The 521.68 cm^{-1} band has relatively narrow Q branches but because of its low intensity the P side of the band is largely lost in the fine structure of the much stronger 370.70 cm^{-1} band. Only two P_{QK} branches can be identified. The absorption at 530.4 cm^{-1} is due to R_{Q_0} which again is narrowed because the 1sJ0 level is involved. The computed J dependence of R_{Q_0} is; $R_{Q_0}(J) = 530.7-4.2\times10^{-3}\ J(J+1)+6.6\times10^{-6}\ J^2(J+1)^2$. In this case, the predicted halfwidth (roughly 0.6 cm^{-1}) is somewhat less than observed (1.2 cm^{-1}) but it must be remembered that the theory does not include vibration-rotation interactions.

The absorption at 549.4 cm^{-1} is somewhat puzzling. A possible explanation for it is that the narrow peak is not part of a Q branch but is due to P and R branch lines similar to those in the background piling up on the broad absorptions produced in this region by R_{Q_1} of this band and P_{Q_1} of the 557.84 cm^{-1} band.

Figures 7 and 8 show that the seven bands discussed above account for nearly all major absorptions with the notable exceptions of the fairly strong absorptions at 251.3 cm^{-1} and 269.4 cm^{-1}. The other band assignments demand that the transition 2s → 2a occur at 206.60 cm^{-1} and it is therefore in a position to contribute to these absorptions. In order to get an estimate of the relative intensity of this and other bands, the following calculations were made.

From analysis of the microwave data, Leacock (15) has shown that it is a good approximation to write the dipole moment of H_2O_2 as $\mu = \mu_o \cos x/2$, that is, as the resultant of two dipoles along the OH bonds. The squared value of the matrix element of cos x/2 between the states $n\tau$ and $n'\tau'$ is therefore proportional to the probability for a transition from the state $n\tau$ to the state $n'\tau'$. These matrix elements were evaluated by the computer. The relative band intensities were then found by including the appropriate frequency and Boltzmann factors. Table XI lists these band intensities relative to the 370.70 cm^{-1} band.

TABLE XI

CALCULATED RELATIVE BAND INTENSITIES

Band	Intensity
242.76	2.01
116.51	0.62
370.70	1.00
198.57	0.37
557.84	0.16
521.77	0.09
206.60	0.19
223.6*	0.09

*Calculated fromthe hindering potential.

The 206.60 cm^{-1} band is seen to have one-half the intensity of the

198.57 cm^{-1} band (which is more than would result from the Boltzmann and frequency factors alone). It is probably not sufficient to account for all of the absorption of 251.3 and 269.4 cm^{-1}. However, part of the absorption at 251.3 cm^{-1} may be due to R_{Q_7} of the 116.51 cm^{-1} band which is calculated to occur at 251.0 cm^{-1} in which case the 206.60 cm^{-1} band might account for the remaining absorption. In regard to the absorption at 269.4 cm^{-1}, it is interesting to note that if the transition 2a → 3s occurred at 224.6 cm^{-1} instead of at 223.6 cm^{-1} as predicted by the theoretical potential, and if ν_{3s} were 9.01 cm^{-1}, then R_{Q_2} of this band would occur at 269.4 cm^{-1}. There is a good possibility that this is the case since this value for ν_{3s} is in line with the progressive decrease observed for $\nu_{n\tau}$ and the difference in the conjectured and computed band centers is only 1.0 cm^{-1}. In fact, the predicted value might well be somewhat too low since the band at 206.60 cm^{-1} is predicted at 206.0 cm^{-1}. According to Table XI, the 2a → 3s band should have one-half the intensity of the 206.60 cm^{-1} band.

Table XII lists the Q branch positions for the 206.60 cm^{-1} band computed from the level constants of Table VIII, the Q branch positions for a band at 224.6 cm^{-1} computed using ν_{3s} = 9.01 cm^{-1}, and the frequencies of the absorption peaks closest to these values. The spectrum is seen to favor the presence of these bands with not inappreciable intensity and it is suggested that the absorptions at 251.3 and 269.4 cm^{-1} are due largely to them.

TABLE XII

CALCULATED Q BRANCH POSITIONS FOR BANDS AT 206.6 CM^{-1} AND 224.6 CM^{-1} AND POSSIBLE EXPERIMENTAL POSITIONS

Q Branch	206.6 cm^{-1} Band		224.6 cm^{-1} Band	
	Calc	Obs	Calc	Obs
R_{Q_5}	304.4	*	322.3	322.4
R_{Q_4}	286.8	286.9	304.8	*
R_{Q_3}	269.3	269.4	287.2	286.9
R_{Q_2}	251.6	251.3	269.4	269.4
.				
.				
.				
P_{Q_3}	160.8	160.7	179.1	179.1
P_{Q_4}	142.4	142.2	160.8	160.7

*Broad absorption centered at about 305.4 cm^{-1}.

It is remarkable, perhaps, that the Q branches from so many different bands overlap so closely. It might be noted that the 3s → 3a transition is predicted to fall at 232 cm^{-1} so that its weak Q branches should not add any intensity to the absorptions at 251.3 and 269.4 cm^{-1}.

4.3 DISCUSSION OF THE GROUND STATE DATA

As indicated earlier, V(x), r_{OO}, r_{OH}, and the OOH angle have been chosen on the basis of their fit to W_{nT}, β_{Os}, ν_{Os}, and γ_{Os}. The present work yields only W_{nT} and ν_{Os} with good accuracy. We consider here

the best values for β_{0s} and γ_{0s} from other data. Redington, Olsen, and Cross (11) have analyzed the 2650 cm^{-1} OOH angle bending combination band in hydrogen peroxide, $\nu_2+\nu_6$, using a slightly asymmetric top treatment. An important feature of this band is that it is not doubled. The vibration is of symmetry species B (antisymmetric under the operation C_2) so that the internal level selection rules are s → s and a → a as shown in Figure 13. The lack of doubling must be interpreted then as a very nearly exact overlap of the two transitions s → s and a → a due to effectively the same hindered rotation splitting in the excited vibrational state as in the ground state. As a result, the ground state rotational constants obtained from an analysis of this band will be an average of those of the 0s and 0a levels. The present theory predicts that $\nu_{0s}-\nu_{0a}$ = +.006 cm^{-1}, $\beta_{0s}-\beta_{0a}$ = .0000 cm^{-1}, and $\gamma_{0s}-\gamma_{0a}$ = -.002 cm^{-1}. This latter difference, which is about 12% of γ_{0s} makes the interpretation of the asymmetry value obtained by Redington et al., somewhat uncertain. On the other hand, their determination of the ground state coefficient of J(J+1) using lines from the R_{Q3} sub-band should be reasonably precise according to the present theory. Examination of the energy level formulae for K = 3 and K = 4 given earlier shows that to a good approximation, the interaction of levels of different n can be neglected. These levels then have the form of those for a slightly asymmetric top (which Redington et al., assumed to be the case) with the coefficient of J(J+1) being $\beta_{n\tau}-1/2\ |\delta_{n\tau}^{n\tau'}|^2/\gamma_{n\tau}$. This coefficient, therefore, corresponds to

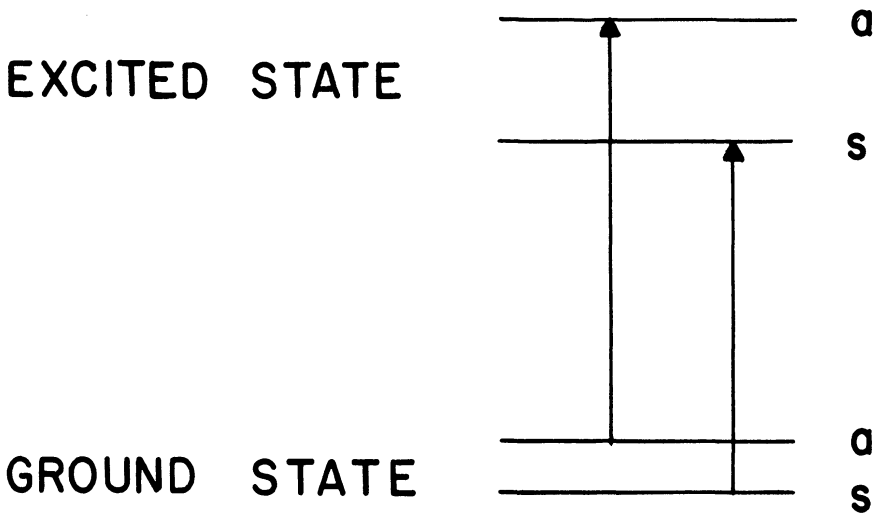

Figure 13. Species B vibration transitions.

their $(B+C)/2$. Since $(B+C)/2$ is predicted to be identical (for all practical purposes) for both components of the ground state, their value of .8562±.001 cm^{-1} for $(B+C)/2$ should be reliable. β_{0s} or β_{0a} then equals .8564±.001 cm^{-1} after insertion of the matrix elements for δ^{02}_{01}, δ^{04}_{03}, and ν_{0s} from Table V

Using the above value of β_{0s}, γ_{0s} can be obtained from the microwave data. The two microwave lines identified by Massey and Bianco (6) are shown in the level diagram of Figure 14. (The quantum numbers are $n\tau JK_{\pm}$ in that order). Lines 1 and 2 occur at 14,829.5 and 37,517.6 Mc/sec, respectively. Addition of these two frequencies gives the equation 1.746 $cm^{-1} = 2\beta_{0s} - 2\gamma_{0s} - 3|\delta^{02}_{01}|^2/\nu_{0s}$. β_{0s} = .8564 cm^{-1}, $|\delta^{02}_{01}|^2 = 3.3\times10^{-3}\ cm^{-1}$ (see Table V) and ν_{0s} = 9.209 cm^{-1}, then yield γ_{0s} = -.017±.001 cm^{-1}. The "ground state asymmetry" quoted by Redington et al., of -.0178 cm^{-1}±.0005 cm^{-1} thus corresponds more closely to γ_{0s} than to γ_{0a}. (For a γ_{0s} of -.017 cm^{-1}, the predicted value of γ_{0s} is only -.015 cm^{-1} as Table V shows.) The ground state splitting can now also be obtained from the microwave data. It is, $W_{0a} - W_{0s}$ = 11.43±.01 cm^{-1}.

For ground state values of $A-(B+C)/2$ and D_K, Redington et al., obtained 9.212 cm^{-1} and 7.5×10^{-4} cm^{-1}, respectively. This value of D_K seems incompatible with the value 4.4×10^{-4} cm^{-1} obtained in this work. However, examination of their plot of the combination differences discloses that $A-(B+C)/2$ = 9.205 cm^{-1} and $D_K = 5\times10^{-4}$ cm^{-1} seem to be equally good values and these agree quite well with the present data.

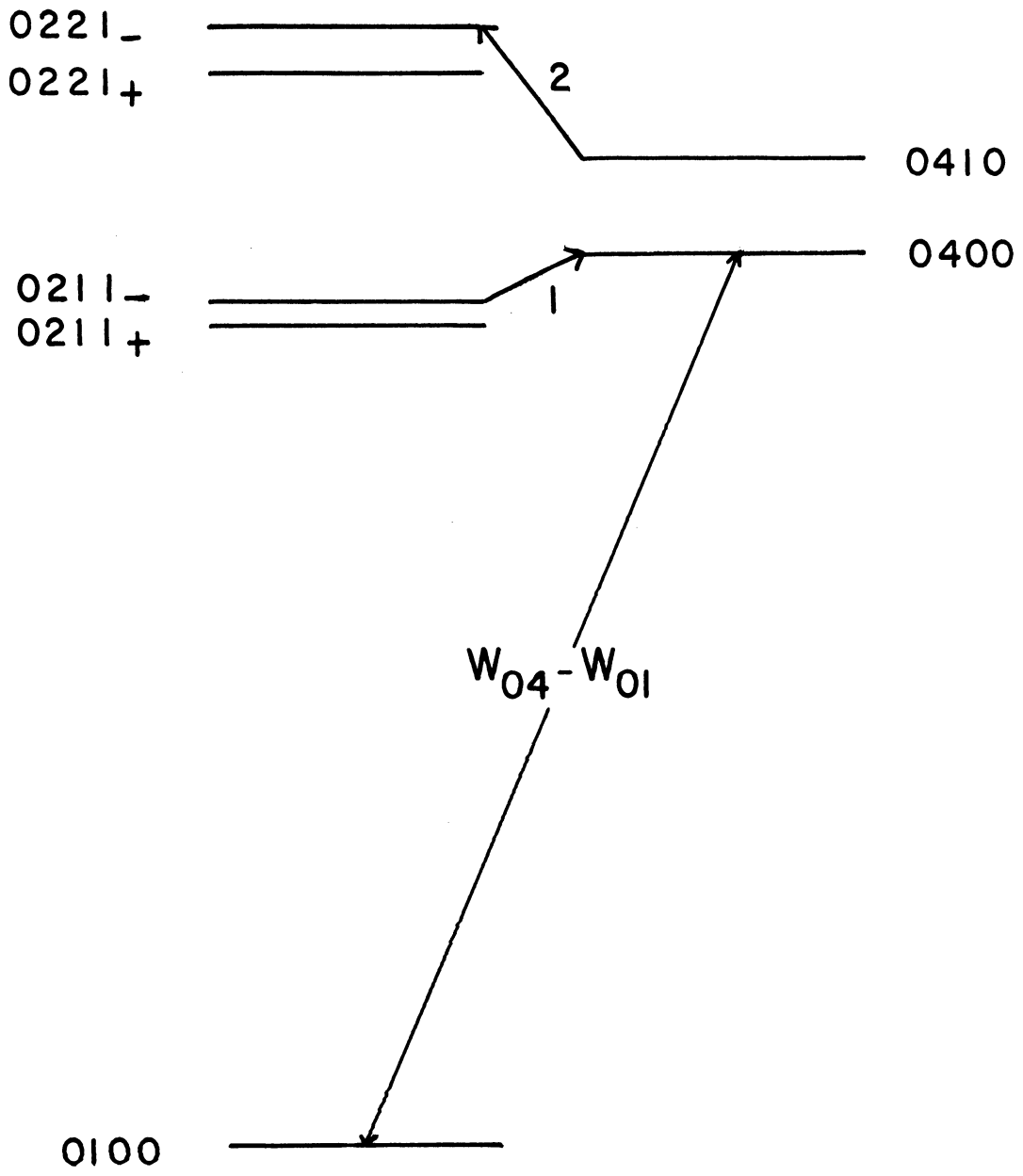

Figure 14. Microwave lines 1 and 2.

Although Redington et al., lacked a knowledge of the hindering potential, their choices for r_{OO}, r_{OH}, and the OOH angle, as noted earlier, reproduce the ground state matrix elements within their experimental error when used with the hindering potential obtained here. One of the reasons for this is that $(B+C)/2$ and $A-(B+C)/2$ do not depend strongly on the internal angle x. They chose as a fourth parameter a fixed value of the internal angle. By assuming an O-H distance of 0.950 A^{o} they determined that an internal angle of 119.8^{o}, an O-O distance of 1.475 A^{o} and an O-O-H angle of 94.8^{o} would be consistent with their rotational constants. As it turns out, the cosine of 119.8^{o} is very close to the expectation value of cos x in the ground state Os. This explains why very nearly the same rotational constants are obtained using the present theory and Redington et al.[1], values for r_{OO}, r_{OH} and the O-O-H angle. This agreement is somewhat accidental, however, since the angle needed for the "fixed" molecular structure in the Oa state is only 114^{o}, due to the slightly different asymmetry of that state. This points out that the dihedral angle of H_2O_2 loses its significance because of the dynamics of the internal motion.

V. COMMENTS

The separation of the Hamiltonian for internal and overall rotation from the five ordinary vibrational degrees of freedom which hydrogen peroxide possesses was justified on the basis of the fact that these vibrations are considerably higher in frequency than are internal rotations. The result of such a separation is that the values determined for the hindering potential coefficients and the coefficients of $\alpha(x)$, $\nu(x)$, etc., are their effective values in the ground vibrational state rather than their equilibrium values. To explicitly take into account interaction of the vibrations with the internal and overall rotations, it would be necessary to include in $V(x)$ and the inertial terms $\alpha(x)$, $\nu(x)$, etc., their dependence on the normal coordinates of the vibrations. Because the observed values for $\nu_{n\tau}$ decrease more rapidly with increasing internal energy than is predicted by the present theory, a more complete treatment could result in some revision of the effective potential coefficients. However, since the vibration-rotation interactions appear to be small as evidenced by the quite good agreement between the present theory and the experimental results, any change in the coefficients of the effective hindering potential should also be small.

The fact that the Q branch widths in the hindered rotation bands are generally greater than predicted is also a result of interaction of the vibrations with the internal and overall rotations as is the

term D_K which is necessary to correct the Q branch positions. With the incomplete band analysis obtained here, it is not possible to get a good estimate of any higher order J dependent interaction terms. Because the dependence of the hindering potential on the normal coordinates can not be calculated, such terms must be determined experimentally. In this connection, it is difficult to see which higher order terms in J and K could be assigned to the overall rotational structure of the various internal levels to account for the appearance of the 242.76 cm^{-1} band. As mentioned, in this band P_{Q_3}, P_{Q_1}, and R_{Q_2} have widths consistent with those predicted but all higher K Q branches are apparently broader than predicted by several wavenumbers. The difficulty arises because both the internal levels involved in this band are involved in other bands whose Q branches are generally less than one wavenumber in halfwidth (if K = 1 is excluded) with no appreciable dependence of this halfwidth on K. It is possible that the appearance of the 242.76 cm^{-1} band is deceptive and that with the strong overlap from other bands in this region its Q branches merge with other Q branches and possibly "pile-ups" of P and R lines to form broad absorptions. This explanation would not be acceptable however, unless the 242.76 cm^{-1} band has a considerably lower intensity than predicted (see Table XI) otherwise P_{Q_4}, R_{Q_4}, and R_{Q_6} would surely be observable. There is some evidence for only moderate intensity for this band as its relatively narrow P_{Q_3} and R_{Q_2}

branches appear similar in strength to those of the 198.57 cm^{-1} band and the latter is predicted to have only about one-fifth the intensity. The true nature of the 242.76 cm^{-1} band could possibly be discovered if an order of magnitude improvement in resolution were available although the large number of bands present make it problematical that a complete band analysis could be achieved.

In so far as the effective hindering potential is concerned, no attempt was made to add a V_4 term for a more perfect fit to the observed levels. Our feeling on this point is that the approximations made in the theory do not justify one to expect a much better fit to the data than has been realized. It might be noted that a two term potential leaves discrepancies in the upper states of several cm^{-1} if the ground state splitting is to be closely fitted.

Some indication of the sensitivity of the barrier heights to the bond lengths and angles of the molecule is given by the effect of a slight change in α_o. α_o is approximately $4(\nu_{0s}+\beta_{0s})$ and is, therefore, determined primarily by the moments of inertia. Its experimental uncertainty is about 0.02 cm^{-1}. A change in α_o of this amount can be balanced by changes of about 10 cm^{-1} in the cis barrier and 1 cm^{-1} in the trans barrier to leave approximately the same internal level structure.

Determination of the internal rotation level structure in the isotopic molecules HDO_2 and D_2O_2 would provide an interesting check on

the effective hindering potential obtained here and perhaps give some information on the vibration-hindered rotation interactions. The only data presently available on the internal rotation level structure of these molecules are the microwave spectra of a mixture of the two isotopes (8). At the time of this writing. Leacock (15) was in the process of analyzing these spectra. First indications are that the observed splittings are quite closely calculated by the hindering potential presented here.

BIBLIOGRAPHY

1. Penney, W. G. and Sutherland, G. B. B. M., J. Chem. Phys. 2, 492 (1934).

2. Zumwalt, L. R and Giguère, P. A., J. Chem. Phys. 9, 458 (1941).

3. Lu, Chia-Si, Hughes, E. W. and Giguère, P. A., J. Am. Chem. Soc. 63, 1507 (1941).

4. Giguère, P. A., J. Chem. Phys. 18, 88 (1950).

5. Bain, O. and Giguère, P. A., Can. J. Chem. 33, 527 (1955).

6. Massey, J. T. and Bianco, D. R., J. Chem. Phys. 22, 442 (1954).

7. Massey, J. T. and Hart, D. W., J. Chem. Phys. 23, 942 (1955).

8. Massey, J. T., Beard, C. I. and Jen, C. K., J. Mol. Spect. 5, 405 (1960).

9. Hunt, R. H. and Peters, C. W., Ohio State Symposium on Molecular Structure and Spectroscopy, June 1961.

10. Chin, D. and Giguère, P. A., J. Chem. Phys. 34, 690 (1961).

11. Redington, R. L.. Olsen, W. B. and Cross, P. C., J. Chem. Phys. 36, 1311 (1962).

12. Randall, H. M. and Firestone, F. A., Rev. Sci. Inst. 9, 404 (1938).

13. McCubbin, T. K., Johns Hopkins University O N R Report, Cont. N5-ORI-166.

14. Burkhard, D. G., J. Chem. Phys., 23, 1405 (1955).

15. Leacock, R. A., University of Michigan Thesis (to appear shortly).

16. Koehler, J. S. and Dennison, D. M., Phys. Rev. 57, 1006 (1940).

17. Hirota, E., J. Chem. Phys. 28, 839 (1958).

AD UNCLASSIFIED

The University of Michigan, Office of Research Administration, Ann Arbor Michigan. The Determination of the Hindered Motion in Hydrogen Peroxide from Its Far Infrared Spectrum, by Robert H. Hunt. June 1963. 69p. incl. illus. tables, 17 refs. ORA Report 03640-2-T (Contract No. AF 19 (604)-6125) UNCLASSIFIED

The hindered rotation in the hydrogen peroxide molecule has been studied by means of the absorption of the vapor in the region from 15 to 700 cm^{-1}. The spectrum was obtained with a vac-

(over) UNCLASSIFIED

AD UNCLASSIFIED

The University of Michigan, Office of Research Administration, Ann Arbor Michigan. The Determination of the Hindered Motion in Hydrogen Peroxide from Its Far Infrared Spectrum, by Robert H. Hunt. June 1963. 69p. incl. illus. tables, 17 refs. ORA Report 03640-2-T (Contract No. AF 19 (604)-6125) UNCLASSIFIED

The hindered rotation in the hydrogen peroxide molecule has been studied by means of the absorption of the vapor in the region from 15 to 700 cm^{-1}. The spectrum was obtained with a vac-

(over) UNCLASSIFIED

AD UNCLASSIFIED

uum grating monochromator with an average resolution of 0.3 cm^{-1}. Analysis of seven hindered rotation bands yielded the positions of the first five excited hindered rotation levels. Relative to the ground state these levels occur at 11.43, 254.2, 370.7, 569.3, and 775.9 cm^{-1}. These levels are closely calculated by the hindering potential (in cm^{-1}), $V(x) = 993 \cos x + 636 \cos 2x + 44 \cos 3x$. This potential has a cis barrier of 2460 cm^{-1}, a trans barrier of 386 cm^{-1}, and a potential minimum 111.5° from the cis configuration.

UNCLASSIFIED

AD UNCLASSIFIED

uum grating monochromator with an average resolution of 0.3 cm^{-1}. Analysis of seven hindered rotation bands yielded the positions of the first five excited hindered rotation levels. Relative to the ground state these levels occur at 11.43, 254.2, 370.7, 569.3, and 775.9 cm^{-1}. These levels are closely calculated by the hindering potential (in cm^{-1}), $V(x) = 993 \cos x + 636 \cos 2x + 44 \cos 3x$. This potential has a cis barrier of 2460 cm^{-1}, a trans barrier of 386 cm^{-1}, and a potential minimum 111.5° from the cis configuration.

UNCLASSIFIED

AD UNCLASSIFIED

The University of Michigan, Office of Research Administration, Ann Arbor Michigan. The Determination of the Hindered Motion in Hydrogen Peroxide from Its Far Infrared Spectrum, by Robert H. Hunt. June 1963. 69p. incl. illus. tables, 17 refs. ORA Report 03640-2-T (Contract No. AF 19 (604)-6125) UNCLASSIFIED

The hindered rotation in the hydrogen peroxide molecule has been studied by means of the absorption of the vapor in the region from 15 to 700 cm^{-1}. The spectrum was obtained with a vac-

(over) UNCLASSIFIED

AD UNCLASSIFIED

The University of Michigan, Office of Research Administration, Ann Arbor Michigan. The Determination of the Hindered Motion in Hydrogen Peroxide from Its Far Infrared Spectrum, by Robert H. Hunt. June 1963. 69p. incl. illus. tables, 17 refs. ORA Report 03640-2-T (Contract No. AF 19 (604)-6125) UNCLASSIFIED

The hindered rotation in the hydrogen peroxide molecule has been studied by means of the absorption of the vapor in the region from 15 to 700 cm^{-1}. The spectrum was obtained with a vac-

(over) UNCLASSIFIED

AD UNCLASSIFIED

uum grating monochromator with an average resolution of 0.3 cm^{-1}. Analysis of seven hindered rotation bands yielded the positions of the first five excited hindered rotation levels. Relative to the ground state these levels occur at 11.43, 254.2, 370.7, 569.3, and 775.9 cm^{-1}. These levels are closely calculated by the hindering potential (in cm^{-1}), $V(x) = 993 \cos x + 636 \cos 2x + 44 \cos 3x$. This potential has a cis barrier of 2460 cm^{-1}, a trans barrier of 386 cm^{-1}, and a potential minimum 111.5° from the cis configuration.

UNCLASSIFIED

AD UNCLASSIFIED

uum grating monochromator with an average resolution of 0.3 cm^{-1}. Analysis of seven hindered rotation bands yielded the positions of the first five excited hindered rotation levels. Relative to the ground state these levels occur at 11.43, 254.2, 370.7, 569.3, and 775.9 cm^{-1}. These levels are closely calculated by the hindering potential (in cm^{-1}), $V(x) = 993 \cos x + 636 \cos 2x + 44 \cos 3x$. This potential has a cis barrier of 2460 cm^{-1}, a trans barrier of 386 cm^{-1}, and a potential minimum 111.5° from the cis configuration.

UNCLASSIFIED

AD

UNCLASSIFIED

The University of Michigan, Office of Research Administration, Ann Arbor Michigan. The Determination of the Hindered Motion in Hydrogen Peroxide from Its Far Infrared Spectrum, by Robert H. Hunt. June 1963. 69p. incl. illus. tables, 17 refs. ORA Report 03640-2-T (Contract No. AF 19 (604)-6125) UNCLASSIFIED

The hindered rotation in the hydrogen peroxide molecule has been studied by means of the absorption of the vapor in the region from 15 to 700 cm^{-1}. The spectrum was obtained with a vac-

(over)

UNCLASSIFIED

AD

UNCLASSIFIED

The University of Michigan, Office of Research Administration, Ann Arbor Michigan. The Determination of the Hindered Motion in Hydrogen Peroxide from Its Far Infrared Spectrum, by Robert H. Hunt. June 1963. 69p. incl. illus. tables, 17 refs. ORA Report 03640-2-T (Contract No. AF 19 (604)-6125) UNCLASSIFIED

The hindered rotation in the hydrogen peroxide molecule has been studied by means of the absorption of the vapor in the region from 15 to 700 cm^{-1}. The spectrum was obtained with a vac-

(over)

UNCLASSIFIED

AD

UNCLASSIFIED

uum grating monochromator with an average resolution of 0.3 cm^{-1}. Analysis of seven hindered rotation bands yielded the positions of the first five excited hindered rotation levels. Relative to the ground state these levels occur at 11.43, 254.2, 370.7, 569.3, and 775.9 cm^{-1}. These levels are closely calculated by the hindering potential (in cm^{-1}), $V(x) = 993 \cos x + 636 \cos 2x + 44 \cos 3x$. This potential has a cis barrier of 2460 cm^{-1}, a trans barrier of 386 cm^{-1}, and a potential minimum 111.5° from the cis configuration.

UNCLASSIFIED

AD

UNCLASSIFIED

uum grating monochromator with an average resolution of 0.3 cm^{-1}. Analysis of seven hindered rotation bands yielded the positions of the first five excited hindered rotation levels. Relative to the ground state these levels occur at 11.43, 254.2, 370.7, 569.3, and 775.9 cm^{-1}. These levels are closely calculated by the hindering potential (in cm^{-1}), $V(x) = 993 \cos x + 636 \cos 2x + 44 \cos 3x$. This potential has a cis barrier of 2460 cm^{-1}, a trans barrier of 386 cm^{-1}, and a potential minimum 111.5° from the cis configuration.

UNCLASSIFIED

AD UNCLASSIFIED

The University of Michigan, Office of Research Administration, Ann Arbor Michigan. The Determination of the Hindered Motion in Hydrogen Peroxide from Its Far Infrared Spectrum, by Robert H. Hunt. June 1963. 69p. incl. illus. tables, 17 refs. ORA Report 03640-2-T (Contract No. AF 19 (604)-6125) UNCLASSIFIED

The hindered rotation in the hydrogen peroxide molecule has been studied by means of the absorption of the vapor in the region from 15 to 700 cm^{-1}. The spectrum was obtained with a vac-

(over) UNCLASSIFIED

AD UNCLASSIFIED

The University of Michigan, Office of Research Administration, Ann Arbor Michigan. The Determination of the Hindered Motion in Hydrogen Peroxide from Its Far Infrared Spectrum, by Robert H. Hunt. June 1963. 69p. incl. illus. tables, 17 refs. ORA Report 03640-2-T (Contract No. AF 19 (604)-6125) UNCLASSIFIED

The hindered rotation in the hydrogen peroxide molecule has been studied by means of the absorption of the vapor in the region from 15 to 700 cm^{-1}. The spectrum was obtained with a vac-

(over) UNCLASSIFIED

AD UNCLASSIFIED

uum grating monochromator with an average resolution of 0.3 cm^{-1}. Analysis of seven hindered rotation bands yielded the positions of the first five excited hindered rotation levels. Relative to the ground state these levels occur at 11.43, 254.2, 370.7, 569.3, and 775.9 cm^{-1}. These levels are closely calculated by the hindering potential (in cm^{-1}), $V(x) = 993 \cos x + 636 \cos 2x + 44 \cos 3x$. This potential has a cis barrier of 2460 cm^{-1}, a trans barrier of 386 cm^{-1}, and a potential minimum 111.5° from the cis configuration.

UNCLASSIFIED

AD UNCLASSIFIED

uum grating monochromator with an average resolution of 0.3 cm^{-1}. Analysis of seven hindered rotation bands yielded the positions of the first five excited hindered rotation levels. Relative to the ground state these levels occur at 11.43, 254.2, 370.7, 569.3, and 775.9 cm^{-1}. These levels are closely calculated by the hindering potential (in cm^{-1}), $V(x) = 993 \cos x + 636 \cos 2x + 44 \cos 3x$. This potential has a cis barrier of 2460 cm^{-1}, a trans barrier of 386 cm^{-1}, and a potential minimum 111.5° from the cis configuration.

UNCLASSIFIED